Mapping the Energy Cascade in the North Atlantic Ocean: The Coarse-Graining Approach

HUSSEIN ALUIE

Department of Mechanical Engineering, and
Laboratory for Laser Energetics, University of Rochester, Rochester, New York

MATTHEW HECHT

Computational Physics and Methods (CCS-2), Los Alamos National Laboratory, Los Alamos, New Mexico

GEOFFREY K. VALLIS

College of Engineering, Mathematics and Physical Science, University of Exeter, Exeter, United Kingdom

ABSTRACT

A coarse-graining framework is implemented to analyze nonlinear processes, measure energy transfer rates, and map out the energy pathways from simulated global ocean data. Traditional tools to measure the energy cascade from turbulence theory, such as spectral flux or spectral transfer, rely on the assumption of statistical homogeneity or at least a large separation between the scales of motion and the scales of statistical inhomogeneity. The coarse-graining framework allows for probing the fully nonlinear dynamics simultaneously in scale and in space and is not restricted by those assumptions. This paper describes how the framework can be applied to ocean flows. Energy transfer between scales is not unique because of a gauge freedom. Here, it is argued that a Galilean-invariant subfilter-scale (SFS) flux is a suitable quantity to properly measure energy scale transfer in the ocean. It is shown that the SFS definition can yield answers that are qualitatively different from traditional measures that conflate spatial transport with the scale transfer of energy. The paper presents geographic maps of the energy scale transfer that are both local in space and allow quasi-spectral, or scale-by-scale, dynamics to be diagnosed. Utilizing a strongly eddying simulation of flow in the North Atlantic Ocean, it is found that an upscale energy transfer does not hold everywhere. Indeed certain regions near the Gulf Stream and in the Equatorial Countercurrent have a marked downscale transfer. Nevertheless, on average an upscale transfer is a reasonable mean description of the extratropical energy scale transfer over regions of $O(10^3)$ km in size.

1. Introduction

Flow in the ocean is complex and very inhomogeneous, characterized by large-scale currents and a vast number of eddies. While much of the time-mean kinetic energy (KE) is concentrated in narrow intense currents such as the Gulf Stream and Kuroshio, a substantial fraction of the total KE is found at smaller scales in the time-varying flow, largely at the mesoscale, where the size of eddies is established by Earth's rotation and the ocean's stratification, with an important scale being the Rossby radius of deformation. The nature of the coupling between features spanning these scales, from the Rossby radius of deformation up to that of the large-scale mean flow, has long been of oceanographic interest. Our incomplete knowledge of the mechanisms that act to couple the mesoscale to the large-scale circulation, and of the pathways through scales below the mesoscale by which energy is dissipated, has hindered our ability to fully account for the ocean's KE budget. There are additional reasons to engage in such study. From the perspective of modeling, one must understand what processes are of fundamental importance if those processes are liable to be compromised within the model,

ⓐ Denotes content that is immediately available upon publication as open access.

Corresponding author: Hussein Aluie, hussein@rochester.edu

as is often the case for processes involving mesoscale eddies (e.g., Ringler et al. 2013; Zanna et al. 2017; Pearson et al. 2017).

An enduring paradigm for oceanic energy pathways between large-scale and mesoscale flow (Gill et al. 1974; Rhines 1975; Salmon 1978, 1980; Smith and Vallis 2002; Vallis 2006; Ferrari and Wunsch 2009) is based on baroclinic instability and homogeneous quasigeostrophic (QG) turbulence theory. At large horizontal scales, there is a source of potential energy (PE), caused by the wind and surface heat fluxes, that drives mesoscale eddies via baroclinic instability. The instability converts large-scale PE into KE at about the Rossby deformation scale of $R_d \approx 50–100$ km. From this scale R_d, much of the KE, at least in this idealized model, undergoes some form of inverse cascade to larger scales. This paradigm is of course highly idealized, whereas the World Ocean is irregular, highly inhomogeneous and constrained by topography and complex boundaries and, importantly, is not fully described by the QG equations. Even within the realm of QG dynamics, barotropic instabilities can arise to transfer energy downscale. One of the main objectives of this paper is to understand if and how this classical paradigm might apply in a more realistic situation, and as a first step we probe directly the KE transfer between scales in a comprehensive, strongly eddying ocean model. Specifically, we analyze the energy transfer across scales at various geographic locations, such as in strong currents, near continental boundaries, and near the equator.

Some intriguing and important work has already been done to examine the flow of energy between different spatial scales in the oceans. For example, the work of Scott and Wang (2005), Arbic et al. (2013), and Tulloch et al. (2011) represents largely successful attempts to characterize turbulent scale transfer as observed from altimetry and generated within models and the extent to which those energy transfers conform to two-dimensional geostrophic turbulence. This and all previous oceanographic analyses, however, have been generated using tools from turbulence theory that rely upon an assumption of statistical homogeneity or, at least, a large-scale separation between the eddying scales of motion and the scales over which the statistics vary.

In this work, we try to relax this assumption by implementing a filtering approach that is mostly novel to large-scale physical oceanography but is well-established in other fluid dynamics disciplines (e.g., Germano 1992; Meneveau 1994; Eyink 1995c; Chen et al. 2003; Aluie 2011; Rivera et al. 2014). The approach is very general, mathematically exact, and based on a coarse-graining framework that can probe the dynamics of length scales at any geographic location and any instant of time, without relying on assumptions of homogeneity or isotropy. It can be used to analyze nonlinear processes, detect and measure energy transfer rates between oceanic structures, and map out energy pathways from ocean altimetry and model data. This paper presents an implementation of coarse-graining analysis for the quantification of oceanic energy flow across spatial scales. Our results indicate that the consequences of the assumption of statistical homogeneity embedded in the traditional tools used for the analysis of turbulence can be substantial when applied in the context of oceanic flows. Whereas our results are in many places in reasonable agreement with those from the traditional method, they are different from the results of traditional analyses in a number of energetic regions, indicating that the assumption of homogeneity is, in those places, not justifiable.

Based on the evidence shown below, coarse-graining is found to be a viable method for exploring the degree to which the generally accepted geostrophic model for such pathways is valid in the ocean and for studying the contribution of various nonlinear mechanisms to the transfer of energy (or potential enstrophy) across scales, such as baroclinic and barotropic instabilities, barotropization, Rossby wave generation, and internal wave generation and breaking. The method can also be applied to smaller scales where the geostrophic assumptions are not generally valid.

From the technical standpoint, this paper aims to introduce and prove the feasibility of the coarse-graining method in physical oceanography. The hope is that it would enable the community to start mapping the energy pathways in the ocean, to identify the sources and sinks acting at different scales, and to quantify the power rates at which they generate or dissipate energy. The application of the method in this paper is restricted to data from an eddy-resolving OGCM, thus allowing us to probe the interaction of mesoscale eddies with the large scales. However, we can also apply the method to simulations that resolve submesoscale processes to probe the interaction of mesoscale and submesoscale eddies with unbalanced motion, such as gravity waves, and dissipative processes. Indeed, the rather general applicability of the method can help lead to a determination of the power requirements to sustain turbulence and mixing, and the overall pathway of energy from source to sink, in the ocean.

This paper is organized as follows: Section 2 introduces the coarse-graining method in some detail and how we apply it to our data. Section 3 discusses the main results of this paper, and section 4 offers a comparison of this work with previous studies that have

tackled these problems. The paper concludes with section 5, which summarizes the main results and offers ideas on potential future work and new research questions that we believe the coarse-graining technique makes feasible.

2. The coarse-graining method

To understand how energy travels through a system, both geographically and with respect to scales (which we shall refer to as spatially and spectrally, respectively), we use a ''coarse-graining'' or ''filtering'' framework that is unusual in large-scale physical oceanography but has become well-established in other fields. It is rooted in a common technique in the mathematical analysis of partial differential equations (e.g., Strichartz 2003; Evans 2010). It was first introduced to the field of turbulence by Leonard (1974) in the context of large-eddy simulation (LES) modeling. The method was further developed mathematically by Eyink (1995a,b, 2005) to analyze the physics of scale coupling in turbulence. It has been utilized in several fluid dynamics applications, ranging from direct numerical simulations (DNS) of turbulence (e.g., Piomelli et al. 1991; Vreman et al. 1994; Aluie and Eyink 2009) to 2D laboratory flows in a shallow tank (e.g., Chen et al. 2006; Kelley and Ouellette 2011; Liao and Ouellette 2015; Fang and Ouellette 2016) and in soap films (e.g., Rivera et al. 2003; Chen et al. 2003; Rivera et al. 2014) to experiments of turbulent jets (Liu et al. 1994) and flows through a grid (Meneveau 1994), through a duct (Tao et al. 2002), in a water channel (Bai et al. 2013), and in turbomachinery (e.g., Chow et al. 2005; Akbari and Montazerin 2013). Moreover, the framework has been extended to rotating stratified flows (Aluie and Kurien 2011), magnetohydrodynamics (Aluie 2017b), and compressible turbulence (e.g., Aluie et al. 2012) and as a framework for parameterizing convection (Thuburn et al. 2018). The schematic in Fig. 1 summarizes the main idea behind the method.

The technique allows for a direct quantification of the strong (or weak) nonlinear coupling between different scales. For example, it allows one to measure the amount and sense (upscale or downscale) of energy being exchanged between different scales at every point **x** in the domain, at every instant in time t. It is a very general approach to analyzing complex flows, the rigorous foundation of which was developed by Germano (1992) and Eyink (1995c, 2005) to analyze the fundamental physics of scale interactions in turbulence. The method allows for probing the dynamics simultaneously in scale and in space and is not restricted by usual assumptions of homogeneity or isotropy. This makes it

ideally suited for studying, on the entire globe, oceanic flows with complex continental boundaries. We have recently developed and generalized the approach to account for the spherical geometry of the flow (Aluie 2017a, manuscript submitted to *Nonlinearity*), with this work being its first implementation in a realistic geophysical system.

a. Coarse-grained fields

The essence of the method is relatively straightforward. For any scalar field $f(\mathbf{x})$, a coarse-grained or (low pass) filtered field, which contains modes at length scales $>\ell$, is defined as

$$\overline{f}_\ell(\mathbf{x}) = G_\ell * f, \tag{1}$$

where $*$ is a convolution, and $G_\ell(\mathbf{r})$ is a normalized kernel (or window function) so that $\int d^2\mathbf{r}\, G_\ell(\mathbf{r}) = 1$. Operation (1) may be interpreted as a local space average over a region of diameter ℓ centered at point **x**. Notice that $\overline{f}_\ell(\mathbf{x})$ has scale information ℓ as well as space information **x**. An example of a kernel G_ℓ is the top-hat kernel:

$$H_\ell(\mathbf{r}) = \begin{cases} A^{-1}, & \text{if } |\mathbf{r}| < \ell/2. \\ 0, & \text{otherwise}. \end{cases} \tag{2}$$

In a flat (Euclidean) 2D domain, the normalization area is $A = (\pi\ell^2)/4$, whereas on Earth's spherical surface, $A = 2\pi R^2[1 - \cos(\ell/2R)]$, where R is Earth's radius. It might be possible to use more general anisotropic kernels to distinguish between zonal and meridional scales, for example. For simplicity, we restrict ourselves to isotropic kernels in this paper and defer such refined analysis to future work. Moreover, while the filtering can be done in all three dimensions, here we focus on the analysis of horizontal scales and filter using 2D kernels to study the scale transfer.

We can also define a complementary high-pass filter that retains only modes at scales $<\ell$ by

$$f'_\ell(\mathbf{x}) = f(\mathbf{x}) - \overline{f}_\ell(\mathbf{x}), \tag{3}$$

which also retains spatial information as a function of **x** and scale information as a function of ℓ. In the rest of our paper, we shall omit subscript ℓ whenever there is no risk of ambiguity.

The scale decomposition in (1) and (3) is essentially a partitioning of scales in the system into large ($\gtrsim\ell$) and small ($\lesssim\ell$). Such a decomposition of the instantaneous flow in the North Atlantic into two sets of scales is shown in Fig. 2, which makes plain two key advantages
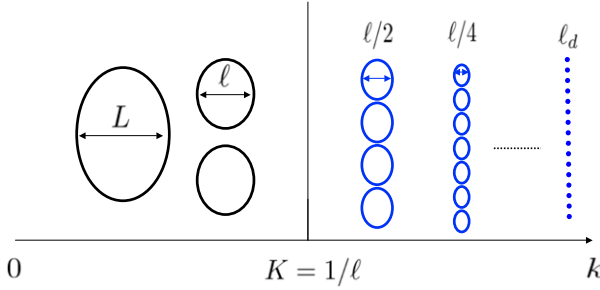
FIG. 1. The coarse-graining approach. The system's size is L, the largest scale. Below the viscous dissipation scale ℓ_d, the dynamics is linear and modes are uncoupled. The dynamics over the entire scale range $L \geq \ell \geq \ell_d$ is given from a numerical simulation or an experiment. Scales are then partitioned (postprocessing) into large and small. Length ℓ represents the smallest scale that is resolved after coarse graining. Scales $<\ell$ (blue) are averaged out.

of the method: (i) an ability to vary the partitioning scale ℓ to gain insight into the geographic location of different oceanic flow structures and (ii) an applicability to single snapshots, thereby allowing, for example, the generation of movies of the flow at any set of length scales.

While the simultaneous resolution of both spatial and scale information of a field $\mathbf{u}(\mathbf{x})$ afforded by filtering is useful, other decompositions, such as with wavelet transforms, can serve a similar purpose. [In fact, wavelets can be used within our approach with the proper choice of filtering kernel $G_\ell(\mathbf{r})$.] Other studies have used filtering for scale decomposition of oceanic data (e.g., O'Neill et al. 2012; Gaube et al. 2015). However, the true potential of the coarse-graining approach as an analysis framework derives mostly from utilizing the dynamical equations, which describe the evolution of various scales. To do so, it is crucial to ensure that the filtering operation [(1)] commutes with spatial derivatives. For example, it must satisfy $\nabla \cdot \overline{\mathbf{u}}_\ell = \overline{\nabla \cdot \mathbf{u}}_\ell$, which guarantees that the filtered flow is incompressible if the original flow satisfies this property, as is the case for the flow in Fig. 2. A simple low-pass filtering, for example, by averaging values at adjacent grid cells or block averaging on the sphere, does not satisfy these conditions and cannot be used for analyzing the dynamics at different scales, as we do here.

The decomposition we use here preserves the fundamental physical properties of the flow, such as its incompressibility, its geostrophic character, and the vorticity present at various scales. This allows for the systematic and rigorous derivation of equations governing any set of scales. For example, since our filtering commutes with spatial derivatives it mathematically guarantees that if one (i) filters the sea surface height (SSH) field first, then computes the velocity, or (ii) computes the velocity first, then filters it, the resultant coarse-grained velocity would be identical.

b. Coarse-grained dynamics and scale coupling

Coarse-grained dynamical equations can be derived to describe the evolution of $\overline{\mathbf{u}}_\ell(\mathbf{x})$ at every point $\mathbf{x}$ in space and at any instant of time. For example, if $\mathbf{u}(\mathbf{x})$ is governed by the rotating Boussinesq equations, then $\overline{\mathbf{u}}_\ell(\mathbf{x})$ is governed by

$$\frac{\partial}{\partial t}\overline{\mathbf{u}}_\ell + \overline{\mathbf{u}}_\ell \cdot \nabla \overline{\mathbf{u}}_\ell = -\frac{1}{\rho_0}\nabla \overline{P}_\ell - f \times \overline{\mathbf{u}}_\ell - \nabla \cdot \overline{\tau}_\ell(\mathbf{u}, \mathbf{u})$$
$$+ \nu \nabla^2 \overline{\mathbf{u}}_\ell + \frac{\overline{\rho}_\ell}{\rho_0}g + \overline{\mathbf{F}}_\ell^{\text{forcing}}. \qquad (4)$$

Here, P is pressure, f is the Coriolis frequency, ν is viscosity, ρ_0 is the reference density, and $\mathbf{F}^{\text{forcing}}$ is forcing such as from winds or tides. Equation (4) is identical to the original unfiltered equation but with an additional contribution from the subfilter stress (oftentimes called subgrid stress in the LES literature):

$$\overline{\tau}_\ell(\mathbf{u}, \mathbf{u}) = \overline{\mathbf{u}\mathbf{u}}_\ell - \overline{\mathbf{u}}_\ell \overline{\mathbf{u}}_\ell, \qquad (5)$$

a tensor representing the forces exerted by scales smaller than ℓ on the larger-scale flow[1] at every location $\mathbf{x}$. In a Navier–Stokes flow, the subfilter term $\overline{\tau}_\ell(\mathbf{u}, \mathbf{u})$ contains all the information needed to quantify the momentum coupling between the two sets of scales, $>\ell$ and $<\ell$. If we have complete knowledge of the dynamics in a simulated or real-life flow, that is, knowing the velocity at every grid point, the subfilter stress can be calculated exactly at every point $\mathbf{x}$ in the domain and at any instant in time t. Furthermore, since (4) describes scales $>\ell$, for arbitrary ℓ (see Fig. 1), we can analyze the spatially resolved nonlinear coupling as a function of scale ℓ.

From the large-scale momentum equation (4), one can derive a KE budget for scales $>\ell$:

$$\frac{\partial}{\partial t}\rho_0 \frac{|\overline{\mathbf{u}}_\ell|^2}{2} + \nabla \cdot \mathbf{J}_\ell^{\text{transport}} = -\Pi_\ell - \rho_0 \nu |\nabla \overline{\mathbf{u}}_\ell|^2 + \overline{\rho}_\ell g \cdot \overline{\mathbf{u}}_\ell$$
$$+ \rho_0 \overline{\mathbf{F}}_\ell^{\text{forcing}} \cdot \overline{\mathbf{u}}_\ell. \qquad (6)$$

See, for example, Germano (1992) for details. Note that what we dub large-scale KE is the KE in the large-scale flow, based on $\overline{\mathbf{u}}_\ell$, rather than the filtered KE itself

---

[1] The (traceless part of the) term $\overline{\tau}_\ell(\mathbf{u}, \mathbf{u})$ is often thought of as a linear diffusive process and modeled as $-2\nu_{\text{turb}}\overline{\mathbf{S}}_\ell$, where $\mathbf{S}$ is the symmetric flow strain tensor. It is important, however, to remember that this is only a model that is often deficient and may sometimes fail altogether.
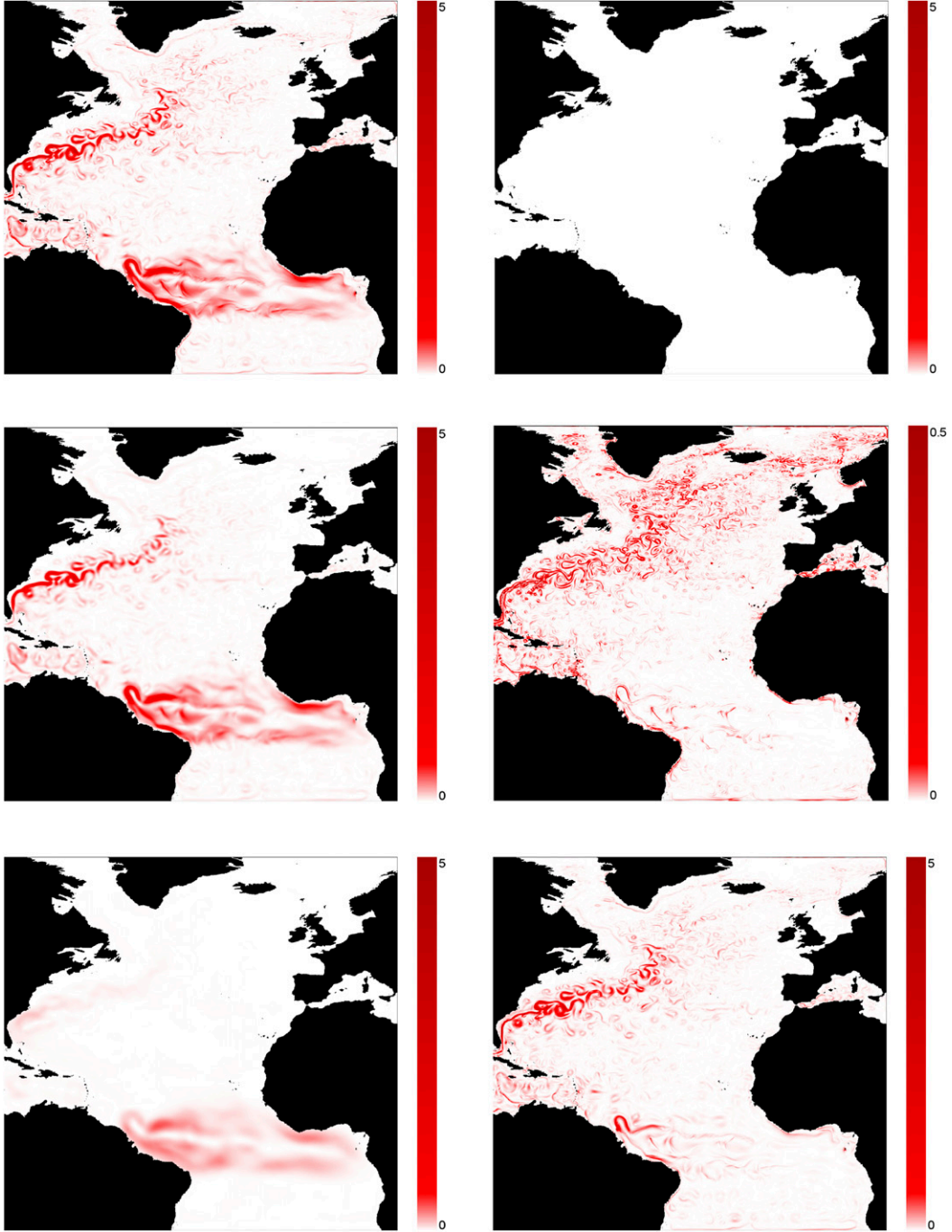
FIG. 2. Our scale decomposition applied to model output (see section 3) at a single instant of time. (left) KE $|\overline{\mathbf{u}}_\ell|^2/2$ (divided by density; $m^2 s^{-2}$) at scales larger than filtering scale ℓ [(1)]. (right) KE, $|\mathbf{u}'_\ell|^2/2$, in the complementary small scales [(3)]. Rows show different filtering scales: (top) unfiltered with $\ell = 0$ km, (middle) filtered at scales $\ell = 100$ km, and (bottom) $\ell = 500$ km. Note the order of magnitude change in color scale to show energy below $\ell = 100$ km in the middle-right panel. When visualizing in this manner, it is important to ensure the grid has sufficient resolution before taking the square of velocity to avoid aliasing effects.

$\rho_0 \overline{|\mathbf{u}|^2}/2$, which *does not* cascade across scales (Germano 1992; Eyink 2005). Here,

$$\mathbf{J}_\ell^{\text{transport}}(\mathbf{x}) = \rho_0 \frac{|\overline{\mathbf{u}}_\ell|^2}{2}\overline{\mathbf{u}}_\ell + \overline{P}_\ell \overline{\mathbf{u}}_\ell - \rho_0 \nu \nabla \frac{|\overline{\mathbf{u}}_\ell|^2}{2}$$
$$+ \rho_0 \overline{\mathbf{u}}_\ell \cdot \overline{\tau}_\ell(\mathbf{u}, \mathbf{u})$$

represents the spatial transport of large-scale KE; the first term is advection by $\overline{\mathbf{u}}_\ell$, the second is transport caused by pressure, the third is diffusion caused by molecular viscosity, and the last term accounts for the role of motion at scales $<\ell$ in transporting KE. The second term on the right-hand side (RHS) of (6) is direct destruction of large-scale KE by molecular viscosity and can be shown mathematically to be negligible at scales $\ell \gg \ell_d$ (e.g., Eyink 2008; Aluie 2013). The third term is conversion from gravitation potential into kinetic energy, the analysis of which yields insight into baroclinic conversion that is believed to drive mesoscale eddies as we shall show in a follow-up work (Sadek et al. 2017). The last term accounts for the direct kinetic energy injection caused by forces such as wind or tides. The first term Π_ℓ is the energy scale transfer or "cascade" term[2] and measures energy transferred from scales $>\ell$ to smaller scale because of nonlinear interactions. This is defined as

$$\Pi_\ell(\mathbf{x}) = -\rho_0 \overline{\mathbf{S}}_\ell : \overline{\tau}_\ell(\mathbf{u}, \mathbf{u}), \qquad (7)$$

which is the large-scale strain tensor $\overline{\mathbf{S}}_\ell = (\nabla \overline{\mathbf{u}}_\ell + \nabla \overline{\mathbf{u}}_\ell^T)/2$, acting against subfilter-scale stress $\overline{\tau}_\ell(\mathbf{u}, \mathbf{u})$. Here, the colon : is a tensor inner product that yields a scalar. In a Navier–Stokes flow, $\Pi_\ell(\mathbf{x})$ contains all the information needed to quantify the exchange of energy between the two sets of scales, $>\ell$ and $<\ell$. Since we have complete knowledge of the dynamics at all scales resolved in a simulation, $\Pi_\ell(\mathbf{x})$ can be calculated exactly at every point $\mathbf{x}$ in the domain and at any instant in time t. This is demonstrated in Fig. 3. It is not possible from simulation, satellite, or field data to capture all scales present in the real ocean. Therefore, computing Π_ℓ is only measuring the dynamical coupling between scales present in the data. It is possible to refine the analysis above by deriving an energy budget within a band of scales as was

shown in Eyink and Aluie (2009); however, the current analysis will suffice for the purpose of this paper.

While spatial maps of $\Pi_\ell(\mathbf{x})$ unravel a wealth of information about the scale dynamics, it is sometimes more insightful to reduce such information by averaging over regions and plotting $\langle \Pi_\ell \rangle$ as a function of the remaining variable ℓ. Figure 4 shows an example of $\langle \Pi_\ell \rangle$ (plotted as a function of $1/\ell$ to make comparison to previous studies easier) that indicates the amount and sense of energy being transferred across different scales.

c. Proper measure of the cascade

In many instances, standard tools that were developed and used in the study of turbulence are only strictly valid to analyze homogeneous isotropic incompressible flows. Consequently, calculations of the energy transfer rates in the ocean that use these tools may give ambiguous results for inhomogeneous flows, as we show in Fig. 3. The problem arises because there are several possible definitions for the cascade term $\Pi_\ell(\mathbf{x})$ in (6), as we now elaborate.

Definition (7) for the scale transfer of energy in budget (6), which we shall call the subfilter-scale flux or SFS flux,[3] is widely used in the LES literature [where $\Pi_\ell(\mathbf{x})$ is often called the subgrid-scale flux or SGS flux], but it is not unique. Another widely used definition is that applied to the ocean by the aforementioned studies and was largely developed in the context of homogeneous turbulence (HT; Frisch 1995):

$$\Pi_\ell^{\text{HT}}(\mathbf{x}) = \rho_0 \mathbf{u} \cdot (\nabla \mathbf{u}_\ell') \cdot \overline{\mathbf{u}}_\ell, \qquad (8)$$

where $\cdot$ is a dot product between a tensor and a vector, which yields a vector. Yet a third possible definition $\Pi_\ell^{\text{uns}}(\mathbf{x}) = \rho_0 [\nabla \cdot (\overline{\mathbf{u}\mathbf{u}}_\ell)] \cdot \overline{\mathbf{u}}_\ell$, which we shall refer to as the unsubtracted flux, was used by Lindborg (2006), Brethouwer et al. (2007), and Molemaker and McWilliams (2010) in idealized geophysically relevant flows. The difference between any two of these definitions is a divergence term $\nabla \cdot (\dots)$, which amounts to a reinterpretation of which terms in budget (6) represent transfer of energy across scales and which terms redistribute (or transport) energy in space $\nabla \cdot \mathbf{J}_\ell^{\text{transport}}$. There is an infinite number of ways to reorganize terms in budget (6) and, thus, an infinite number of possible definitions for the transfer of kinetic energy between scales. This freedom in defining $\Pi_\ell(\mathbf{x})$ can be thought of as a gauge freedom.

---

[2] The term cascade generally implies a spectrally local transfer and therefore is a stronger statement than just transfer, although it is common in physical oceanography to use the two terms synonymously. However, in this manuscript, we henceforth avoid using the term cascade when unwarranted since we are not making any statement about the scale locality of the transfer, which can be diagnosed through a more refined analysis similar to what was done in Eyink and Aluie (2009) and Aluie and Eyink (2009).

---

[3] The term flux in this context denotes a flux of energy across scales, which has units of power per unit volume. It should not be confused with a spatial flux, such as $\mathbf{J}_\ell^{\text{transport}}$ in (6), which has units of power per unit area. Our terminology is borrowed from the turbulence and LES literature.
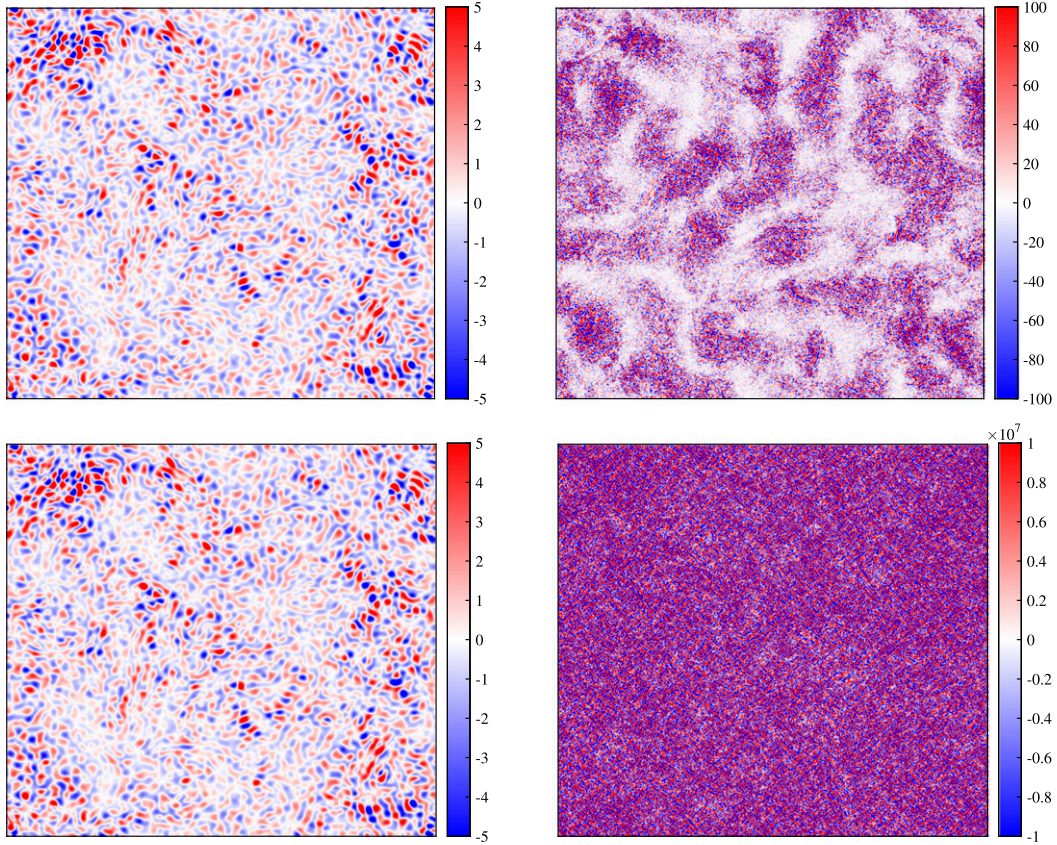
FIG. 3. The energy transfer across scale $\ell = L/30$ (L is the domain size), at a single time instant, at every $\mathbf{x}$. Data are from a 3D triply periodic simulation of homogeneous isotropic turbulence forced at large scales. Red (blue) is energy transferred from scales larger (smaller) than ℓ to scales smaller (larger) than ℓ. Top-left panel uses the SFS cascade measure, which is Galilean invariant, whereas the top-right panel uses the HT definition (Frisch 1995), which is not, yielding an unphysical imprint of the large scales. Bottom two panels measure the energy transfer using the respective definitions after embedding the fluctuations in a uniform mean flow, underscoring the dependence of Π_ℓ^{HT} on the observer's inertial frame of reference.

In a homogeneous flow, spatial averages of all these definitions are equal because their difference is a divergence that is zero: $\langle \nabla \cdot (\ldots) \rangle = 0$. On the other hand, if one considers inhomogeneous flows, such as in the ocean or atmosphere, or if one wishes to analyze the cascade geographically without spatial averaging, then such definitions can differ qualitatively as well as quantitatively. We will now argue that the SFS flux definition (7) is the proper measure of the cascading energy because it satisfies an important physical criterion: Galilean invariance. Using such a criterion to choose the definition of the SFS flux may be thought of as gauge fixing.

GALILEAN INVARIANCE

Galilean invariance is the requirement that a determination of the amount of energy cascading at any given point $\mathbf{x}$ should not depend on the velocity of the observer. In other words, a measurement from a ship

sailing in the Gulf Stream and another from a station on land should register the same amount of energy being exchanged between scales. Kraichnan (1964), Speziale (1985), Germano (1992), and Eyink (2005) all emphasized the importance of Galilean invariance in the context of turbulence, and, more recently, Eyink and Aluie (2009) and Aluie and Eyink (2009) showed that Galilean invariance was necessary for the so-called scale locality of the cascade. There are non-Galilean-invariant terms in our budgets [(6)], but, as is physically natural, they are all associated with spatial transport $\mathbf{J}_\ell^{\text{transport}}$ of energy.

Definition $\Pi_\ell^{\text{HT}}(\mathbf{x}) = \rho_0 \mathbf{u} \cdot (\nabla \mathbf{u}_\ell') \cdot \overline{\mathbf{u}}_\ell$ does not satisfy Galilean invariance. An observer moving at a constant velocity $-\mathbf{U}_0$ relative to the system will measure a flux at point $\mathbf{x}$,

$$\Pi_\ell^{\text{HT}}(\mathbf{x}) = \rho_0 [\mathbf{u} \cdot (\nabla \mathbf{u}_\ell') \cdot \overline{\mathbf{u}}_\ell + \mathbf{u} \cdot (\nabla \mathbf{u}_\ell') \cdot \mathbf{U}_0$$
$$+ \mathbf{U}_0 \cdot (\nabla \mathbf{u}_\ell') \cdot \overline{\mathbf{u}}_\ell + \mathbf{U}_0 \cdot (\nabla \mathbf{u}_\ell') \cdot \mathbf{U}_0],$$
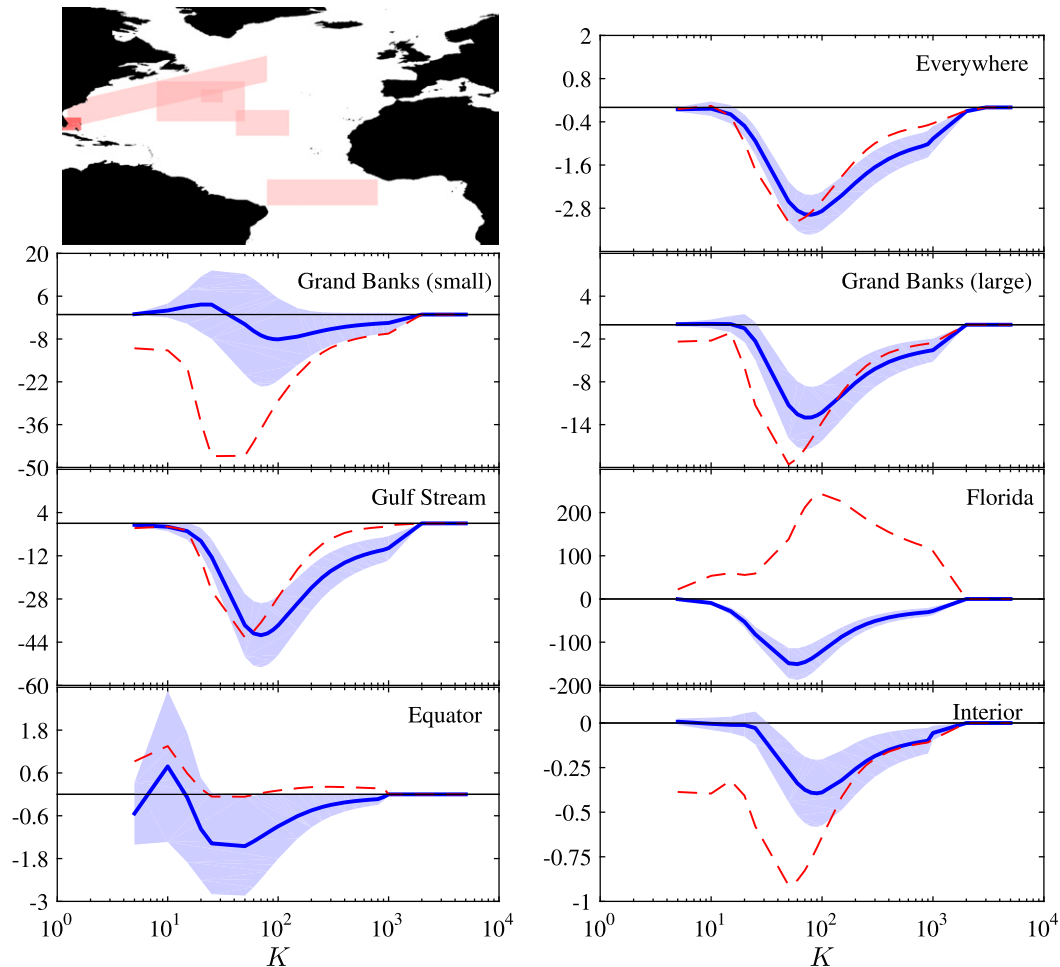
FIG. 4. Spatially averaged SFS flux (solid blue line; W km^{-2} m^{-1}) $\langle \Pi_\ell \rangle$ at the ocean surface as a function of scale $K = 10^4/\ell$ km^{-1}. Here, K is not a wavenumber, just a number proportional to ℓ^{-1}. The uppermost left panel shows the various regions over which $\Pi_\ell(\mathbf{x})$ is averaged. In the remaining panels the transparent blue shade depicts the temporal standard deviation in the SFS flux over a 3-yr period (110 snapshots), while the solid blue line is the temporal average. This is compared to the homogeneous turbulence flux $\langle \Pi_\ell^{\mathrm{HT}} \rangle$ (dashed red) without artificial tapering or boosting. Significant qualitative (and not just quantitative) differences in Florida, the equator, and the Grand Banks where strong mean currents exist (Gulf Stream and North Equatorial Current), sweeping through the box.

such that the amount of energy cascading at an arbitrary location in the flow will be dependent on the frame of reference. For large sweeping speeds $|\mathbf{U}_0|$, the measured cascade becomes proportional to $|\mathbf{U}_0|^2$, as demonstrated in Fig. 3.

On the other hand, both the subfilter stress in (5) and the SFS flux in (7) satisfy Galilean invariance. This property can be directly verified by the reader with elementary algebra and is demonstrated in Fig. 3.

The two cascade measures, visualized in Fig. 3, show very different qualitative and quantitative behavior. The term Π_ℓ^{HT} has a strong dependence on the most energetic structures in the flow, with a conspicuous imprint of the strongest eddies forming the peak of the energy spectrum. To underscore Galilean invariance, we boost the

velocity by a constant $U_0 \hat{\mathbf{x}} = 1000\,\hat{\mathbf{x}}$ m s^{-1} and recalculated the fluxes using both definitions. As expected, the SFS flux Π_ℓ does not change. On the other hand, Π_ℓ^{HT} exhibits an unphysical dependence on the reference frame and is proportional to $O(U_0^2)$.

The idea we are emphasizing is that any definition of a flux, which measures the amount of energy cascading across a scale ℓ, should be Galilean invariant. Otherwise, the amount of energy cascading at a point $\mathbf{x}$ in the flow would depend on the inertial frame of reference of the system, which is unphysical. Disentangling the cascade across scales from spatial transport is especially pertinent when trying to determine the sense of a cascade visually by looking at the evolution of structures. Consider a simple 3D pure Navier–Stokes turbulent

flow in a laboratory tank. If one injects a localized blob of tracer somewhere in the flow, the blob will diffuse and expand. At face value, an observer might be tempted to conclude that the flow (and the tracer) is undergoing an inverse cascade because the size of the blob is growing. However, it is well-known that both energy and tracer variance in a 3D Navier–Stokes flow undergo a cascade to smaller scales (e.g., Pope 2000). The observed expansion is in fact due to spatial transport by turbulence, which is sometimes referred to as turbulent diffusion. If such spatial transport is subtracted by using a reference frame comoving with the local large-scale flow, then the observer would notice that the tracer, which started as a continuous blob, develops fine filaments and becomes fractal (down to the viscous scales), indicating a downscale cascade. This is precisely what the SFS flux definition (7) measures. While Fig. 3 relies on a boosting velocity for the purpose of illustration, we will see below that Galilean invariance proves to be of significance in a number of regions within the North Atlantic Ocean.

3. Results

Since we can probe the dynamics simultaneously in scale ℓ and in space $\mathbf{x}$, we show two types of results below. The first type explores the energy transfer across various scales ℓ, spatially averaging $\langle \Pi_\ell \rangle$ over a region of interest. The region may be very small in geographic extent or very large, encompassing the entire domain. The second type of results we present keeps scale ℓ, across which energy is being transferred, fixed while fully resolving the scale transfer in space. This yields spatial maps of $\Pi_\ell(\mathbf{x})$.

As we mentioned above, it is important to bear in mind that the scale coupling unveiled by our analysis is an exact description of the fully nonlinear dynamics in the simulation, which may be different from that of the real ocean. This is a limitation shared by any qualitative or quantitative analysis done on data, be it from simulations or observations.

We will now present an analysis of the scale transfer in the North Atlantic using OGCM data. Our method can also be applied to observational data, including satellite altimetry and Argo floats. But here we take advantage of the uniform and complete coverage afforded through the use of simulation output in order to establish the effectiveness of the method. We hope that it will then subsequently be applied to observational data.

a. Description of simulation

The simulation we analyze is the 14b case of Bryan et al. (2007). As explained in that paper, this simulation was generated with the POP free-surface, hydrostatic primitive equation code (Dukowicz and Smith 1994) using z coordinates and a full-cell representation of topography. A mercator grid with zonal grid spacing of 0.1° and meridional spacing of 0.1°[sin(latitude)] covered the Atlantic basin from 20°S to 73°N, including the Gulf of Mexico and the western Mediterranean. Toward the northern boundary of the domain, the first internal Rossby radius of deformation becomes poorly resolved, with only one grid cell spanning the Rossby radius at the highest latitudes of the North Atlantic basin (see Fig. 1 of Smith et al. 2000). This important dynamical length scale tends to be adequately resolved, however, at the latitudes of our analysis regions (see our Fig. 4 below for the analysis regions). A 40-level grid was used in the vertical with cell thickness increasing from 10 m at the surface to 250 m in the deep ocean. Biharmonic eddy viscosity ν and diffusivity κ was used, scaled with the cube of the local grid spacing, as

$$\nu = \nu_0 \left(\frac{dx}{dx_0} \right)^3 \tag{9}$$

(and similarly for κ), such that the grid-scale Reynolds number

$$\mathrm{Re}_{\mathrm{grid}} = \frac{U \, dx^3}{\nu_0} \tag{10}$$

is constant for a fixed velocity scale, regardless of location on the grid. Here, $\nu_0 = -1.35 \times 10^{10} \, \mathrm{m^4 \, s^{-1}}$, and the corresponding diffusive coefficient was $\kappa_0 = \nu_0/3$. The Pacanowski and Philander (1981) parameterization of vertical mixing was used with background values of viscosity and diffusivity of 10^{-4} and $10^{-5} \, \mathrm{m^2 \, s^{-1}}$, respectively. A quadratic bottom stress with a drag coefficient of 1.225×10^{-3} was applied.

The experiment was forced with a daily averaged wind stress, computed from ECMWF TOGA surface analyses (derived from operational forecasts and provided on a 1.125° Gaussian grid) for mid-1985 to early 2001. A repeating annual cycle of surface heat flux is prescribed using the Newtonian cooling boundary condition of Barnier et al. (1995) with a penetrative solar radiation flux. A restoring boundary condition is used for surface salinity, damping the model solution toward the Levitus (1982) monthly climatology on a time scale of 1 month. The north and south boundaries of the domain are closed to flow, with temperature and salinity restored to the annual-mean Levitus climatology within 3° wide buffer zones. Details of this and other points of model configuration appear in the earlier paper of Smith et al. (2000).

The model output that we analyze was saved at 10-day intervals over a 3-year period of the simulation, from March 1998 through February of 2001.
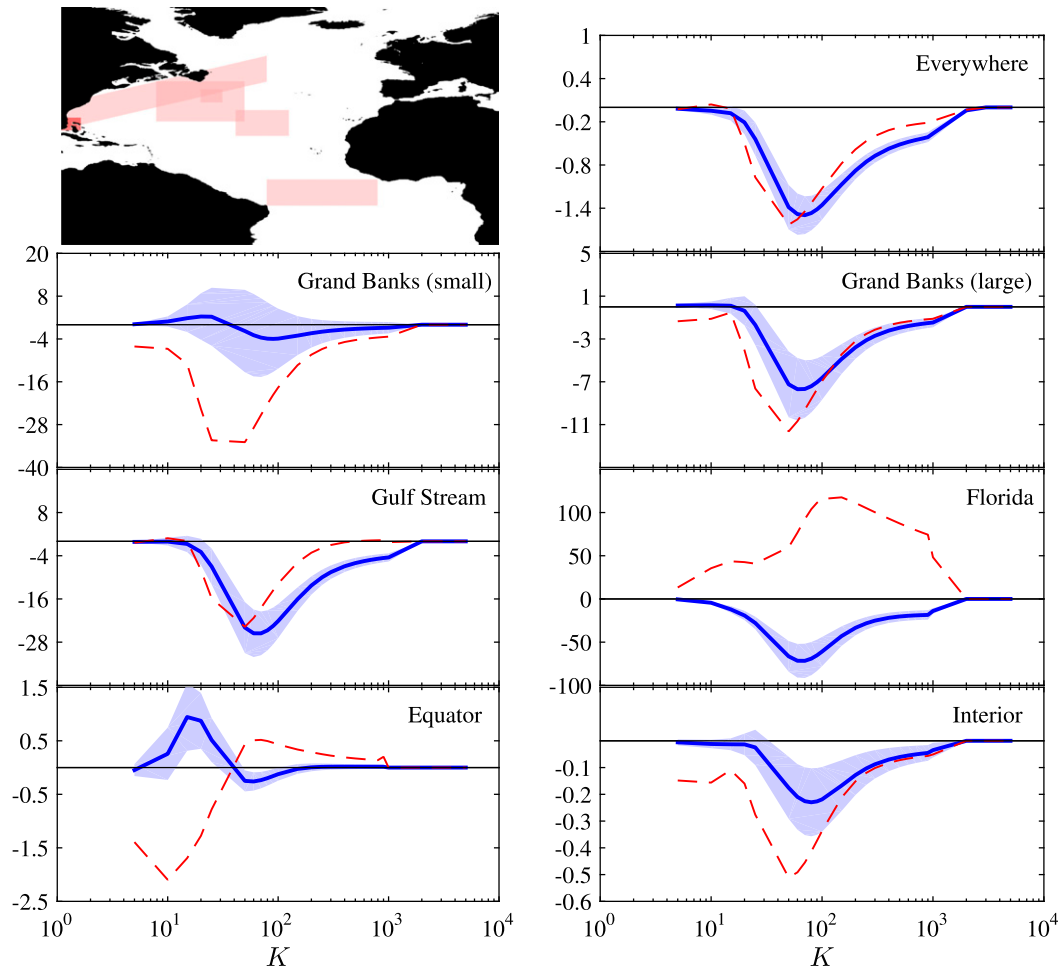
FIG. 5. As in Fig. 4, but at 100-m depth. We again see significant differences between the two measures of energy transfer, especially in Florida, the equator, and the Grand Banks where strong mean currents sweep through the box.

b. Mapping energy scale transfer

Figures 4–7 show the scale transfer at various locations and depths in the ocean as a function of scale ℓ. (The plot is a function of $1/\ell$ to make comparison to previous studies easier.) The depths we have chosen are (i) at the surface to compare to previous results using altimetry data; (ii) at 100-m depth, slightly below the average depth of the mixed layer; (iii) at 500-m depth, within the thermocline; and (iv) at 2000 m within the more weakly stratified depths of the ocean. The regions we have chosen are (i) the entire North Atlantic domain of our data to characterize the scale transfer at the basin scale; (ii) a large region near the Grand Banks, in the Gulf Stream Extension, which overlaps with the region studied in Arbic et al. (2013) to compare with that study; (iii) a smaller region of the Grand Banks, to test the role of region size on the dis/agreement between the SFS and

the HT cascade measures; (iv) a small region east of Florida, within the Gulf Stream, where sweeping effects are very large; (v) a region encompassing most of the Gulf Stream and its extension to measure the scale transfer in a western boundary current system, something that was absent from previous studies and that can be carried out with our coarse-graining approach; (vi) a small region in the Sargasso Sea, at approximately the center of the North Atlantic's subtropical gyre, to measure the scale transfer in a relatively quiescent region within which sweeping effects are negligible; and (vii) an equatorial region, between 5°S and 5°N and 10° and 35°W, that covers the North Equatorial Current and Countercurrent in our simulation and where the geostrophic approximation fails.

Figures 4 and 5 show that HT and SFS are qualitatively different in regions where sweeping effects by
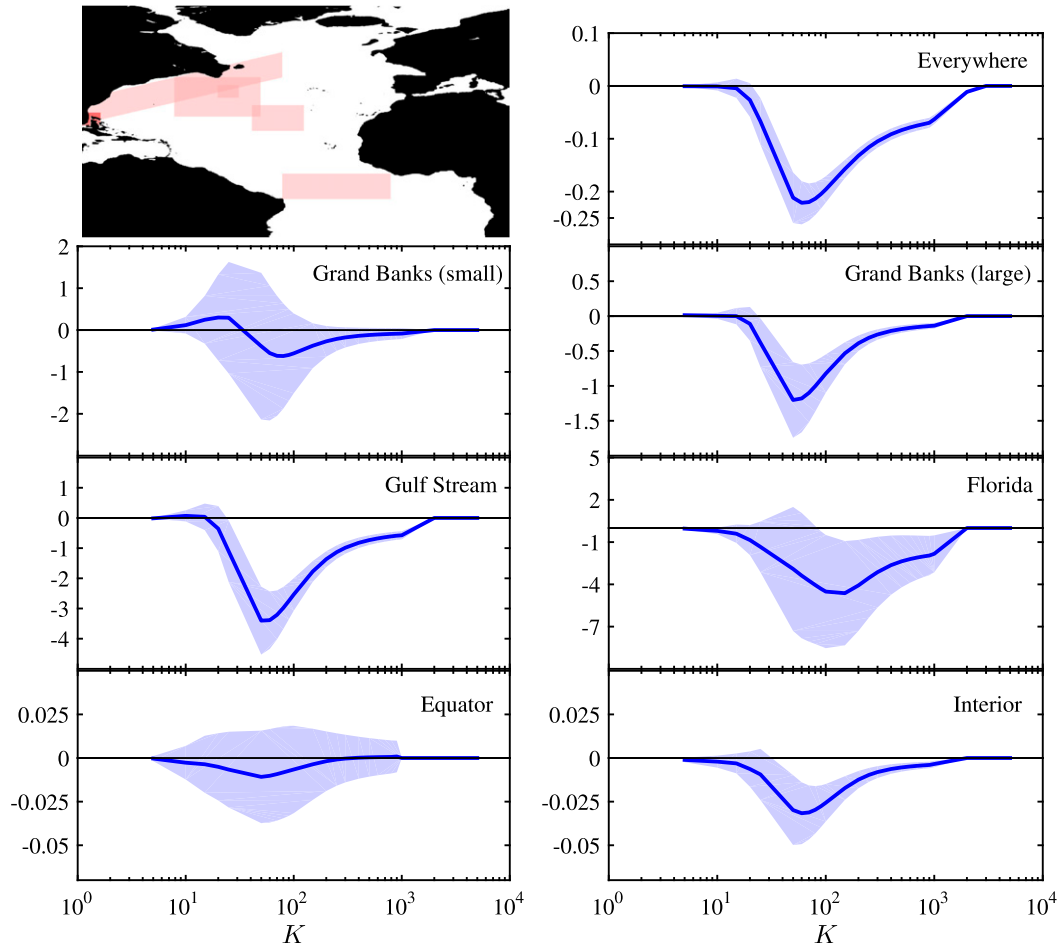
FIG. 6. As in Fig. 4, but 500-m depth. This depth is within the thermocline, where stratification effects are, on average, strongest in the ocean. We notice that the energy transfer across scales is an order of magnitude smaller here than in the mixed layer, near the surface.

mean oceanic current are important, especially in the Florida region, but also in the equator and the small Grand Banks boxes. In the larger Grand Banks region, where the mean Gulf Stream is relatively less dominant, SFS and HT are in qualitative agreement. When averaging over the entire domain, over which mean sweeping effects are exactly zero (zero flow in or out of the domain), the two definitions yield very similar results. From Figs. 4 and 5, we also see that the interior region in the Sargasso Sea is not as homogeneous as one may think, where we find that the HT and SFS definitions agree over scales smaller than 50 km but diverge over larger scales.

Figures 8–10 show geographic maps of interscale energy transfer in the ocean. They are time-averaged over a 3-yr period, which we have checked to be almost identical to 2-yr averaged maps, indicating that the features shown are persistent in time. The maps reveal

intense KE scale transfer taking place in the Gulf Stream and in the North Brazil Current. There is also a weaker but significant scale transfer in most of the North Atlantic, not as visible because of the color map. As one would expect, the scale transfer is significantly stronger in the uppermost layers compared to the deeper ocean.

The qualitative nature of scale transfer differs significantly at various geographic locations and depths. For example, we observe an upscale transfer of energy in the surface equatorial region, where the equatorial flow is from east to west. On the other hand, Figs. 9 and 4 show that in the Equatorial Countercurrent at 100-m depth, the transfer is almost entirely downscale. We note that QG theory is not expected to hold at the equator.

Another prominent feature we observe in Figs. 8 and 9, especially across $\ell = 200$ km at which the transfer peaks, is a strong (dark blue) upscale transfer in the Gulf Stream core east of Florida and the Carolinas. This persists well
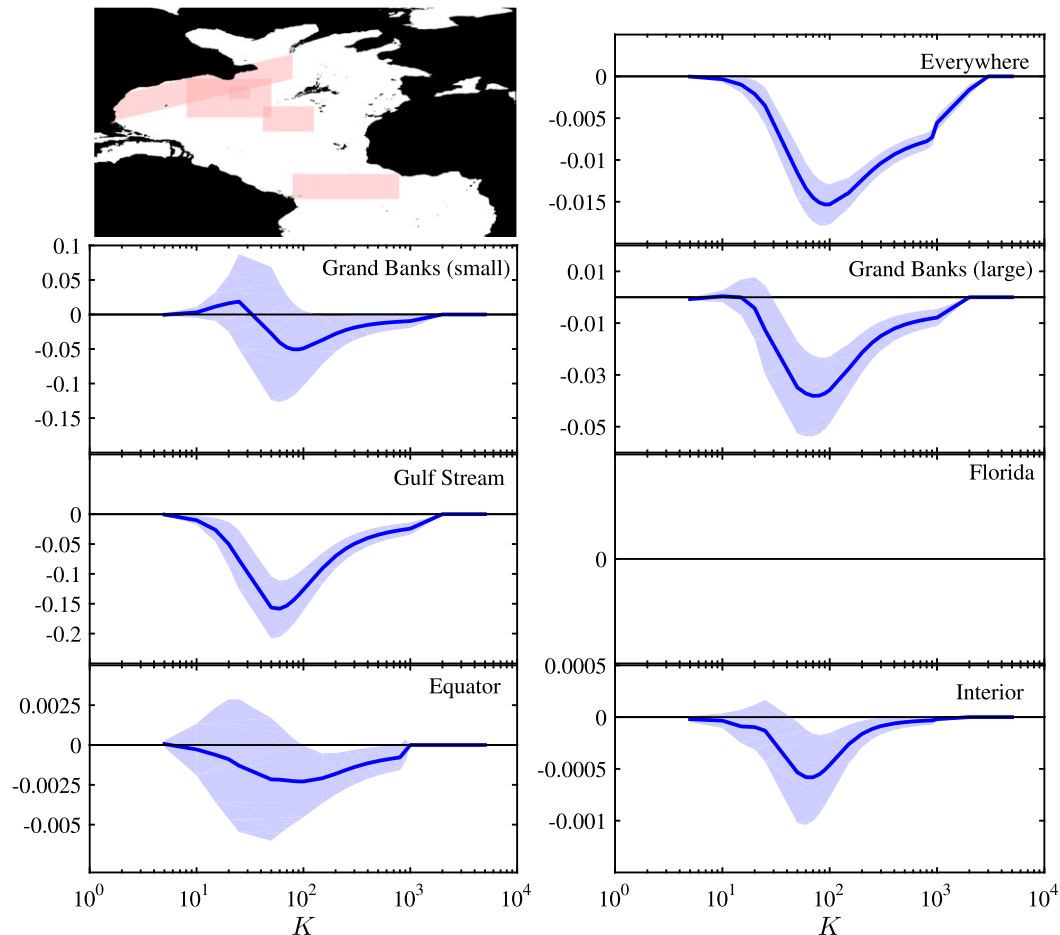
FIG. 7. As in Fig. 4, but at 2000-m depth. This is within the deep ocean, where stratification effects are, on average, weakest in the ocean. We notice that the energy transfer across scales is two orders of magnitude smaller than in the mixed layer, near the surface.

beyond the separation point (Cape Hatteras), indicating that energy is transferred from mesoscale eddies into the Gulf Stream, accelerating and focusing the current. Flanking both sides of this (dark blue) core, we see downscale transfer (red) most probably associated with barotropic instabilities resulting from strong shear. This supports recent eddy–mean flow interaction models that rely on decomposing the flow into mean and fluctuating parts (e.g., Waterman and Jayne 2011). Overall, an up-scale transfer dominates in the Gulf Stream, in general accord with the traditional QG paradigm. A similar pattern, though not as pronounced, exists in the North Brazil Current.

We also observe from Figs. 8 and 9 a persistent red patch in the Gulf Stream as it passes through the Florida Strait just south of the peninsula. This indicates an expenditure of kinetic energy by the Gulf Stream as it traverses the Florida Straight and undergoes a sharp turn northward. This is not necessarily associated with a slowdown in the mean current speed since any loss may be offset by other forcing mechanisms, such as buoyancy or wind forcing. Another northward turn occurs at the Grand Banks, where the North Atlantic current carries subpolar gyre waters farther poleward than anywhere else on Earth. Here, a strongly coherent red core of downscale energy transfer is flanked on both sides by upscale transfer or inverse cascade. An in-depth investigation of these issues is worth pursuing in future work but would take us beyond the scope of this paper.

Figures 8–10 show that the SFS flux, which is a scalar field, seems to be mostly depth-independent at high latitudes. In other words, the pattern of red versus blue in the Gulf Stream, indicating the sense of the energy scale transfer, appears to be nearly the same at the surface, at 100-m depth, and also at 500-m depth, which has practical utility in inferring transfer from surface altimetry data.

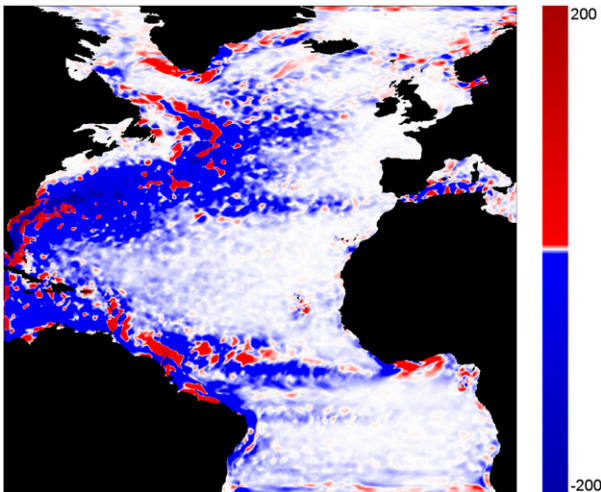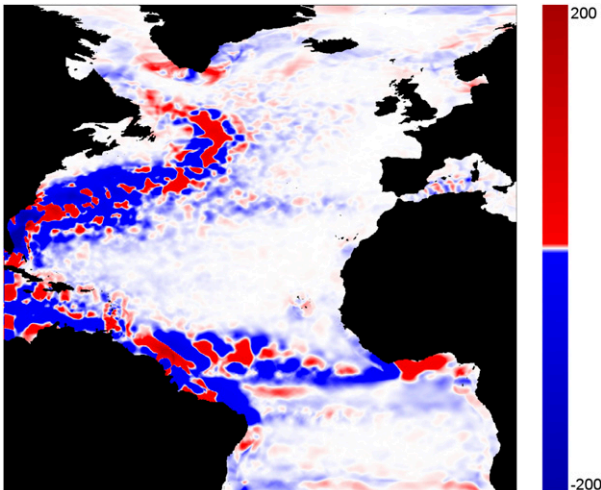We also notice from Figs. 4–7 that the temporal fluctuations in the scale transfer differ as a function of the

FIG. 8. Geographic maps of the interscale energy transfer $\Pi_\ell(\mathbf{x})$ (W km^{-2} m^{-1}) at the surface, time averaged over 3 years (110 snapshots), where (top) $\ell = 400$ km and (bottom) $\ell = 200$ km. The color map used, is not linear; most of the color shown has small values close to zero (white), and some blue/red regions exceed the maximum values on the color bar. We observe a downscale transfer in the current south of Florida, as the Gulf Stream turns northward, possibly indicative of eddy shedding or even just the small scale associated with the sharp turn in the trajectory. We also observe a strong (dark blue) upscale transfer in the Gulf Stream core east of Florida and the Carolinas. This persists well beyond the separation point (Cape Hatteras), indicating that energy is transferred from mesoscale eddies into the Gulf Stream, accelerating and focusing the current. Flanking both sides of this (dark blue) core, we see downscale transfer (red) most probably associated with barotropic instabilities resulting from strong shear. Overall, an upscale transfer dominates in the Gulf Stream, in accordance with QG. A similar pattern, though not as pronounced, exists in the North Brazil Current. The (shallow) North Equatorial Current, which in our simulation is around 5°N, exhibits an upscale energy transfer.
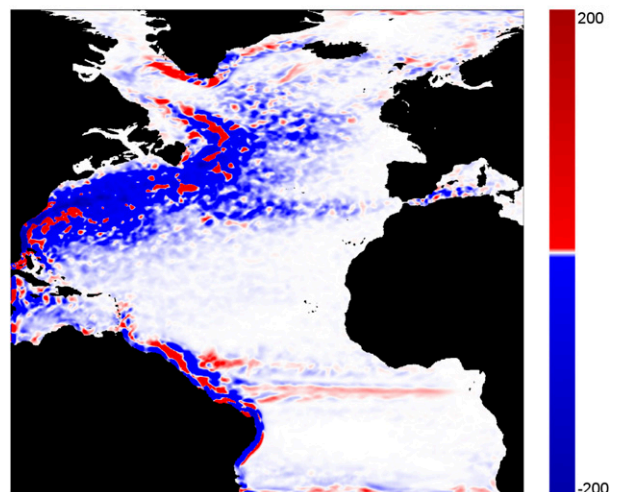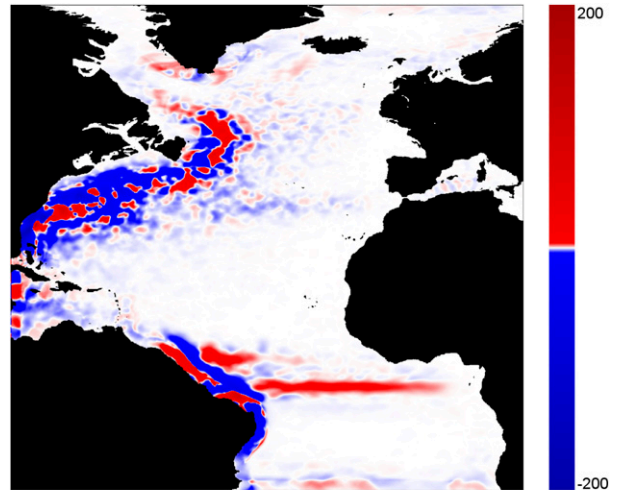
FIG. 9. As in Fig. 8, but at 100-m depth. We notice in the Gulf Stream a pattern similar to that at the surface. In fact, almost the exact red/blue patch patterns that appear at the Gulf Stream surface appear at 100- and 500-m depth (see next Fig. 10), suggesting that $\Pi_\ell(\mathbf{x})$, as a scalar field, is depth independent at high latitudes. On the other hand, we notice that there is a downscale transfer of energy in the Equatorial Countercurrent, which in our simulation, is approximately at 0° and 100-m depth, indicating an obvious departure from the QG model.

averaging box and the nature of the flow within the box. For example, we find that in regions where a relatively strong coherent mean flow exists, such as in the Equatorial Countercurrent at 100-m depth or near Florida, the temporal variation is smaller than in regions that lack a strong coherent mean flow, such as at the equatorial surface, Sargasso Sea, and the small Grand Banks region where the instantaneous sweeping by the Gulf Stream Extension is strong but is not temporally coherent.

A general conclusion we can deduce from Figs. 8–10 is that an upscale energy transfer does not take place everywhere in the ocean, even at the higher latitudes. On the other hand, if we average over large enough regions (of order 10^3 km in size or larger) in the ocean, away from the equator, we find from Figs. 4–7 that the
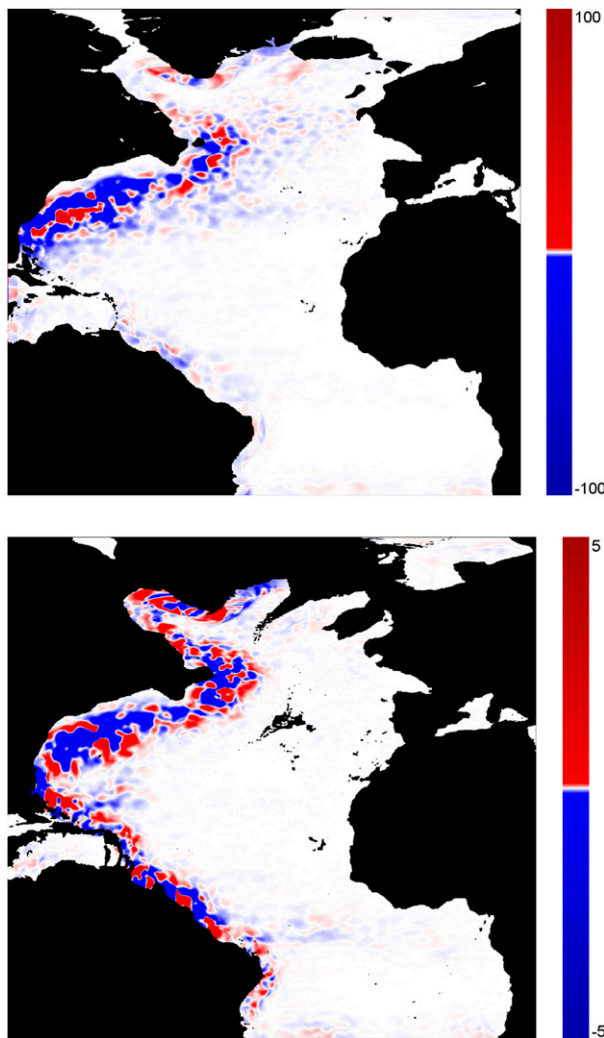
FIG. 10. As in Fig. 8, but at depths of (top) 500 m and (bottom) 2000 m, where $\ell = 400$ km. We notice that within the thermocline in the (top), the scale transfer is weak with the exception of the Gulf Stream, which is known for its deep penetration. The red/blue patch patterns are similar to those appearing at the Gulf Stream surface and at 100 m. It is also clear from the color bar magnitudes of the bottom panel that there is relatively weak scale transfer in the deep ocean.

quasigeostrophic paradigm of an upscale transfer is a qualitatively correct mean description of the energy scale transfer in a basin-averaged sense.

It is well-documented in the homogeneous isotropic turbulence literature (e.g., Chen et al. 2003; Boffetta 2007; Rivera et al. 2014) that the spatial distribution of the SFS flux $\Pi_\ell(\mathbf{x})$ is very different from that of a Gaussian distribution. It is spatially intermittent and characterized by heavy tails, such that $\Pi_\ell(\mathbf{x})$ is small in magnitude almost everywhere in space with only a few spatial regions having very large magnitude (either positive or negative). The net (or spatially averaged) amount of energy cascading across scales $\langle \Pi_\ell \rangle$ is further reduced as a consequence of major

cancellations between upscale and downscale transfer [positive and negative values of $\Pi_\ell(\mathbf{x})$], accentuating the disparity between average and extreme values. In Figs. 8–10 we observe a similar tendency for $\Pi_\ell(\mathbf{x})$ in oceanic flow. Note that the color map we use in the figures, which has units of watts per square kilometer per meter, is not linear. Most of the color shown on the map has small values close to zero (white), while some blue/red regions exceed the maximum values on the color bar. If we were to use a linear color map, we would register white almost everywhere with only a few patches of blue/red in the Gulf Stream. It is therefore important to bear in mind, when visually inspecting the maps in Figs. 8–10, that similar shades of red/blue may have considerably different values.

In Fig. 8, we see that the North Equatorial Current, which is a shallow surface current moving westward and, in our simulation, is at approximately 5°N, exhibits an upscale energy transfer. On the other hand, in Fig. 9, we notice that the Equatorial Countercurrent, which is a deeper eastward-moving current and, in our simulation, is at approximately 100-m depth and along the equator undergoes a downscale transfer of energy, perhaps not unexpectedly since quasigeostrophic dynamics is not valid at the equator. At 500-m depth, we notice from Figs. 6 and 10 that scale transfer is relatively weak with the exception of the Gulf Stream, which is known for its deep penetration. This depth is well below the mixed layer within the thermocline, where stratification effects are strongest in the ocean.

While flow in the upper ocean, above approximately 1500 m, is mostly due to wind forcing, the circulation in the deep ocean is mostly due to buoyancy forcing and the meridional overturning circulation (e.g., Talley et al. 2011). The major western boundary currents, such as the Gulf Stream, are among the more strongly barotropic features and can penetrate all the way to the ocean bottom. Figures 7 and 10 show that the relatively unstratified deep ocean is quiescent, with energy transfer approximately $O(10^2)$ smaller than in the mixed layer. The main activity is along the western boundary where the flow is strongest.

4. Comparison to other techniques

As mentioned in the introduction, there have been several studies published in the literature exploring the transfer of energy between scales (e.g., Scott and Wang 2005; Tulloch et al. 2011; Arbic et al. 2013). These have used somewhat different tools from the turbulence literature than have we (such as the HT definition of flux) and used Fourier transforms to decompose scales in wavenumber space. In this section, we explore some of the differences between these approaches and our own.

a. Tapering and detrending

Using data from either satellites or simulations, the aforementioned studies considered box regions in the ocean that are away from continental boundaries. Since these box domains do not satisfy periodic boundary conditions, the data have to be adjusted before applying FFTs. One standard method in signal processing is periodizing the domain, such that the box is reflected eight times around the original, resulting in a super box that is periodic (Tulloch et al. 2011). Another standard method is to smoothly taper the data to zero near the edges of the box, such that the data become de facto periodic (Scott and Wang 2005; Arbic et al. 2013). Both of these methods can introduce artificial gradients, length scales, spurious acceleration, and flow features not present in the original data, although in some circumstances these effects may be small. Here, we consider only the more widely used method of tapering.

Previous studies relied on the geostrophic velocity obtained from SSH anomalies, which may be considered as streamfunction, ψ. These are related by

$$(u_x, u_y) = (-\partial_y \psi, \partial_x \psi) g/f, \tag{11}$$

where g is gravity, and f is the local Coriolis frequency. To illustrate the effect of tapering in the simplest possible situation, consider a constant streamfunction $\psi = (\text{const.})$ corresponding to a velocity that is identically zero. Tapering ψ would introduce artificial vorticity and spurious length scales that are absent in the original (zero) flow. It should be noted that Scott and Wang (2005) and Arbic et al. (2013) detrended ψ by removing the mean and linear components of ψ before tapering, such that this illustrative example does not apply to those studies.

However, detrending cannot remove all spurious tapering artifacts. This is illustrated in Fig. 11, which shows a 2D flow in a periodic box and computes the true spectral energy flux (top panel of Fig. 11) in the simulation. In a periodic flow, the HT and SFS flux definitions agree since the flow is homogeneous. The middle panel of Fig. 11 shows the flow after detrending and tapering with a window that mimics a Tukey window[4] (e.g., Emery and Thomson 2001). It is clear that despite detrending, spurious flow features and length scales are

introduced solely because of tapering. These artifacts are also reflected in the computed spectral energy flux, which nearly doubles in magnitude and is shifted to larger scales because of the artificial introduction of large-scale flow structures. Even if the flow is homogeneous to begin with, as is the case of this periodic flow, tapering can have a substantial effect. We observe these artifacts (shifts in scale and alteration of the flux magnitude) caused by tapering using several windows (Hann, Tukey, and Tanh) and with different sharpness of the tapering function. While it is common in signal processing, including in physical oceanography (e.g., Emery and Thomson 2001, chapter 5.6.6), to compensate for any reduction in energy caused by windowing by multiplying the Fourier amplitudes by an empirically determined factor, the practice only works (to some extent) for spectra but not for spectral fluxes. This is because the flux is a nonlinear quantity, which corresponds to a convolution in Fourier space. Its value at a certain wavenumber k is determined by modes $k–p$ and p for all wavenumbers p. Therefore, a loss in amplitude at a certain mode can affect the flux at all modes k in a nontrivial way. The flux's response to window functions, unlike the spectrum's response, cannot be determined a priori because it requires knowledge of the phase relations between different modes and not just their amplitudes.

Moreover, if a flow is not detrended, tapering artifacts may become even more pronounced. This is illustrated in the bottom panel of Fig. 11. It shows the tapering effect if the fluctuations are embedded in a mean current (which is not detrended). In this case, the spectral energy flux increases by an order of magnitude and shifts to yet larger scales.

b. Reynolds-averaging approaches

Our coarse-graining approach is also very different from ensemble-averaging or Reynolds-averaging (RANS) frameworks (e.g., Gnanadesikan et al. 2005; Waterman and Jayne 2011) or density-weighted averaging (Young 2012; Maddison and Marshall 2013), whose essential aim is to decompose the flow into a mean and fluctuating components. Several studies have relied on these types of eddy–mean flow decompositions to analyze the energy transfer between the large-scale mean flow and the eddy component of the flow (e.g., von Storch et al. 2012; Chen et al. 2014; Kang and Curchitser 2015; Youngs et al. 2017).

A difference between coarse-graining over RANS is the freedom of the former to choose the specific spatial scales to probe (Fig. 2), which allows us to generate energy transfer maps across any scale (Figs. 8–10), and to quantify the energy scale transfer as a function of scale (Figs. 4–7). RANS frameworks, on the other hand,

---

[4] Our window $W(x, y) = W(x) \times W(y)$, $W(x) = (1/2) - (1/2)\{\tanh[(|x| - 0.8\pi)/0.2]\}$, $(x, y) \in [-\pi, \pi)$ corresponds to a Tukey window with $\alpha = 0.4$ and yields a value of 1 over about two-thirds of the domain in each direction and tapers smoothly to zero over the remaining one-third of the domain. This is similar to what was used in previous studies (e.g., Arbic et al. 2013).
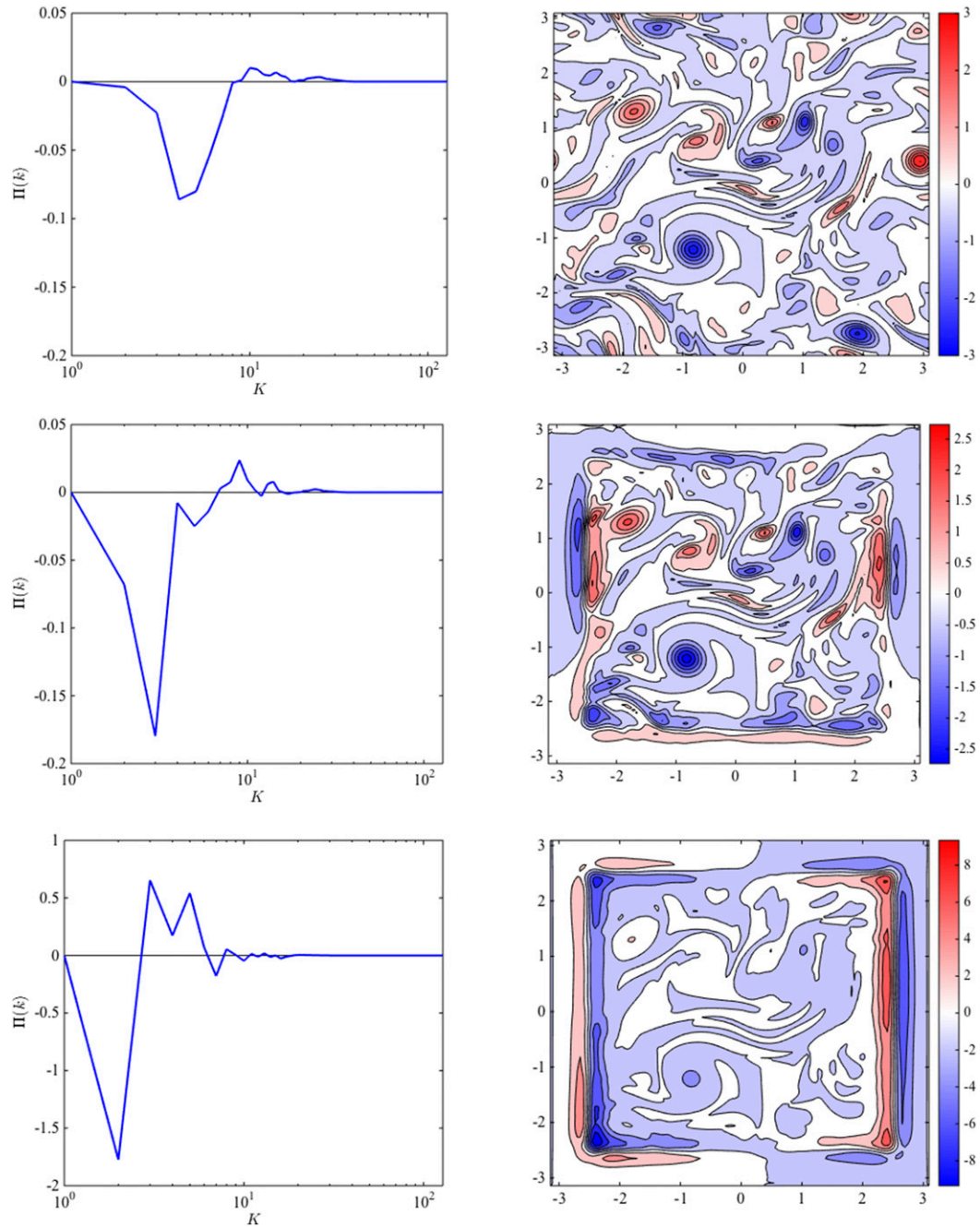
FIG. 11. (left) $\langle \Pi_K \rangle$ as a function of scale $K = 2\pi/\ell$. (right) Vorticity contours. (top) Original ψ_{orig} from a 2D flow with periodic boundaries. (middle) Tapered streamfunction, similar to what was done in Arbic et al. (2013). (bottom) Uniform velocity $\mathbf{u}_0 \hat{\mathbf{i}}$ is added to the original flow before tapering the streamfunction $\psi_{\text{orig}} + U_0 y$, which illustrates the effect of tapering a jet. Even in the absence of a jet in the (middle), we see that tapering introduces artificial vorticity and shear to the flow, along with spurious length scales. This is reflected as a shift in $\langle \Pi_K \rangle$ to larger scales (smaller K), along with significant changes in the magnitude of energy transfer.

usually decompose the flow into mean and fluctuating components without control over spatial scales. Moreover, the RANS description of the flow is inherently statistical in nature, whereas the coarse-graining method

of probing the dynamics is deterministic, allowing us to describe the evolution of scales at every location and at every instant in time. As a result, we are able to generate movies of the evolution of different scales.

However, the two approaches are not mutually exclusive. The RANS framework could in principle be incorporated into the coarse-graining approach since time averaging (or, more generally, ensemble averaging) and spatial filtering are operations that commute with each other. One may choose to ensemble or time average the coarse-grained dynamics, as we have done in Figs. 8–10. Alternatively, one may spatially filter the mean and/or fluctuating components of the flow after having performed a RANS decomposition.

c. Difficulties with our approach

Although our filtering approach does allow us to produce meaningful maps of energy scale transfer in physical space like those in Figs. 8–10, it is not immune from complications. One of these (and that is also a problem with spectral approaches) is that regions close to continental boundaries, and therefore boundary currents, require a choice to be made of boundary treatment. If we were to filter the flow at a location adjacent to land in a standard way the filtering kernel would overlap land points because in order to obtain the coarse-grained velocity $\overline{\mathbf{u}}_\ell(\mathbf{x})$, which is the flow at location $\mathbf{x}$ solely composed of scales larger than ℓ, we need to perform a weighted average of the velocity within a region of radius $\ell/2$ around $\mathbf{x}$, which might include land. A practical choice made in this work is to treat land as water with zero velocity. The diagnostics are then insensitive to whether we treat land points as a solid or as water with an imposed zero velocity, which is consistent with the formulation of OGCMs where land is often treated as a region of zero velocity.

Another trade-off made by using our approach is due to the uncertainty principle, which prevents the simultaneous localization of a kernel in x space and in k space. If we were to use a kernel that is a delta function in x space, then we are not decomposing scales; its Fourier transform is unity, and by multiplying the Fourier transform of the velocity field with the Fourier transform of the kernel, we do not eliminate any modes (a convolution becomes a multiplication in Fourier space). The duality of such a statement is using a kernel that picks out a single Fourier mode, that is, a kernel that is a delta function in k space centered at mode k_0. Then we lose localization in x space since the inverse Fourier transform of such a delta function gives a kernel that is a cosine wave of infinite extent in x space. Therefore, by using a kernel that allows a certain degree of localization in x space, we forfeit the exact localization in k space afforded by Fourier eigenmodes. These trade-offs caused by the uncertainty principle are fundamental to harmonic (or spectral) analysis and therefore the trade-off between spatial and spectral localization cannot be eliminated. However, in our opinion, losing localization in k space is not necessarily detrimental in situations where performing Fourier transforms is not possible, such as in the oceanic setting. Further discussion of these and related matters can be found in standard mathematics references on harmonic analysis (e.g., Stein and Weiss 1971; Krantz 1999; Strichartz 2003; Sogge 2008).

A practical consequence of forfeiting exact spatial localization is that oceanic boundaries become "fuzzy" because of coarse graining. This implies, for example, that coarse-grained velocity $\overline{\mathbf{u}}_\ell$ can be nonzero within a distance $\ell/2$ beyond the continental boundary over land. Therefore, terms in the large-scale energy budget (6), such as Π_ℓ and $\mathbf{J}_\ell^{\text{transport}}$, are only guaranteed to be zero over land a distance $\ell/2$ beyond the boundary. While this aspect of the method may seem undesirable, it is worth bearing in mind that such an effect also occurs in simulations of flow over a coarse grid of cell size $\Delta x = \ell$. The alternative choice is to make the filter kernel change shape as it approaches the boundary, either by making it smaller or making it conform to the boundary, but such a filtering operation will no longer commute with spatial derivatives. As a consequence of this alternative choice of boundary treatment, the coarse-graining operation would no longer preserve the fundamental physical properties of the flow, such as its incompressibility and the vorticity present at various scales. This would prevent us from deriving the large-scale energy budget [(6)], as discussed in section 4a above. To preserve these fundamental properties of the flow after coarse graining, we leave the filter independent of its proximity to the boundary.

We also want to make the reader aware of another issue pertaining to the choice of a kernel. In this work, we have made a practical choice to use a top-hat kernel, (2) above, which has a normalized value of 1 over a circular region of radius $\ell/2$ and zero beyond. In our opinion, this kernel makes the notion of scale more straightforward since it has a well-defined extent in x space. Because of the uncertainty principle, however, it decays slowly in k space and therefore may not be the best kernel to use when Fourier transforms are possible (see Fig. 13 of Rivera et al. 2014). There are many other kernels one could use, such as a Gaussian kernel, which affords more localization in k space (Fig. 13 of Rivera et al. 2014) but less localization in x space, or the Sinc function, which affords the same localization in k space as truncating the Fourier series but has very poor localization in x space and is more costly to implement and use. Such freedom in the kernel choice may be considered as providing flexibility, but it may also be viewed as an arbitrariness in the scale decomposition, which can influence the quantitative nature of the results. Many works have investigated the utility and drawbacks of

different kernels (e.g., Vreman et al. 1994; Domaradzki and Carati 2007; Eyink and Aluie 2009; Rivera et al. 2014). For example, (18) and Fig. 12 of Rivera et al. (2014) discuss the energy and enstrophy fluxes across scales using different kernels. It is therefore important to keep these nuances in mind when interpreting results using coarse-graining, especially when comparing them to results from a purely spectral analysis when Fourier transforms are possible.

5. Conclusions

Understanding the transfer of energy across scales is of fundamental importance in oceanography. Standard methods based on Fourier analysis have provided important results but are limited in their applicability to quasi-homogeneous regions with simple boundary conditions, and the techniques typically require some kind of special treatment at the boundaries. Information about the scales of motion is not inherently tied to a Fourier mode decomposition, as is clear from using wavelet analysis or simply by high- or low-pass filtering in physical space. However, a straightforward application of such filters is insufficient to extract dynamical information, such as the energy transfer across scales that can be revealed only by nontrivial use of the equations of motion in conjunction with the scale decomposition.

In this paper, we have shown that a filtering technique, which we have generalized to use on spherical manifolds, can be used to infer information about the scales of motion and the energy transfer between scales, without being limited by assumptions of homogeneity or by the need to perform the analysis in a domain with simple boundaries. The technique involves a filter in physical space (a convolution with a kernel or window function), such as might be applied to smooth a field, but, moreover, used in such a way that coarse-grained equations of motion in physical space can be derived and cross-scale energy transfer deduced. We have applied the technique, using full spherical geometry, to the results from a high-resolution eddying primitive equation model of the North Atlantic Ocean.

Our method allows us to create geographic maps of the energy transfer. We find that an inverse energy transfer does not take place everywhere in the ocean (Figs. 5–8) or even everywhere in the extratropical ocean. In fact, certain regions are characterized by sustained downscale energy transfer, such as at the sharp northward turn of the Gulf Stream at the Grand Banks, in the flanks of the core of the Gulf Stream, and in the Equatorial Countercurrent. These effects may be due to a local instability of the flow creating smaller scales or

to nongeostrophic effects, and more analysis and results from observed flows will follow in subsequent papers. In any case, with our method, we can clearly identify and locate regions where forward cascade from larger scales energizes the smaller scales, and we can measure the magnitude of that energy transfer.

Despite the presence of regions of significant downscale transfer, we find that if we average over large enough regions, of order 10^3 km in size or larger, away from the equator, an upscale transfer is, in a basin-averaged sense, the dominant description of the energy scale transfer process, confirming the importance of geostrophic processes on the meso- and large scales. Finally, we remark that the tool can also be applied to smaller-scale flows, such as the interaction between mesoscale eddies and gravity waves (Nikurashin et al. 2013) or in principle to microstructure measurements. The tool, however, has its limitations. As discussed in section 4, in order to spatially resolve the scale dynamics, a certain degree of scale localization must be forfeited because of the uncertainty principle.

Our formalism can be applied to flow data from numerical simulations and also from satellite altimetry, as we hope will be demonstrated in future work. Another potential benefit of this method is in the promising area of scale-aware modeling, where the grid resolution can vary in space, thus requiring subfilter models that are attuned to both geographic location and to the local grid scale. The coarse-graining approach provides a natural gateway to developing such scale-aware and space-aware parameterizations.

REFERENCES

Akbari, G., and N. Montazerin, 2013: On the role of anisotropic turbomachinery flow structures in inter-scale turbulence energy flux as deduced from SPIV measurements. *J. Turbul.*, **14**, 44–70, https://doi.org/10.1080/14685248.2013.861073.

Aluie, H., 2011: Compressible turbulence: The cascade and its locality. *Phys. Rev. Lett.*, **106**, 174502, https://doi.org/10.1103/PhysRevLett.106.174502.

——, 2013: Scale decomposition in compressible turbulence. *Physica D*, **247**, 54–65, https://doi.org/10.1016/j.physd.2012.12.009.

——, 2017b: Coarse-grained incompressible magnetohydrodynamics: Analyzing the turbulent cascades. *New J. Phys.*, **19**, 025008, https://doi.org/10.1088/1367-2630/aa5d2f.

——, and G. Eyink, 2009: Localness of energy cascade in hydrodynamic turbulence. II. Sharp spectral filter. *Phys. Fluids*, **21**, 115108, https://doi.org/10.1063/1.3266948.

——, and S. Kurien, 2011: Joint downscale fluxes of energy and potential enstrophy in rotating stratified Boussinesq flows. *Europhys. Lett.*, **96**, 44006, https://doi.org/10.1209/0295-5075/96/44006.

——, S. Li, and H. Li, 2012: Conservative cascade of kinetic energy in compressible turbulence. *Astrophys. J. Lett.*, **751**, L29, https://doi.org/10.1088/2041-8205/751/2/L29.

Arbic, B. K., K. L. Polzin, R. B. Scott, J. G. Richman, and J. F. Shriver, 2013: On eddy viscosity, energy cascades, and the horizontal resolution of gridded satellite altimeter products. *J. Phys. Oceanogr.*, **43**, 283–300, https://doi.org/10.1175/JPO-D-11-0240.1.

Bai, K., C. Meneveau, and J. Katz, 2013: Experimental study of spectral energy fluxes in turbulence generated by a fractal, tree-like object. *Phys. Fluids*, **25**, 110810, https://doi.org/10.1063/1.4819351.

Barnier, B., L. Siefridt, and P. Marchesiello, 1995: Thermal forcing for a global ocean circulation model using a 3-year climatology of ECMWF analyses. *J. Mar. Syst.*, **6**, 363–380, https://doi.org/10.1016/0924-7963(94)00034-9.

Boffetta, G., 2007: Energy and enstrophy fluxes in the double cascade of two-dimensional turbulence. *J. Fluid Mech.*, **589**, 253–260, https://doi.org/10.1017/S0022112007008014.

Brethouwer, G., P. Billant, E. Lindborg, and J.-M. Chomaz, 2007: Scaling analysis and simulation of strongly stratified turbulent flows. *J. Fluid Mech.*, **585**, 343–368, https://doi.org/10.1017/S0022112007006854.

Bryan, F. O., M. W. Hecht, and R. D. Smith, 2007: Resolution convergence and sensitivity studies with North Atlantic circulation models. Part I: The western boundary current system. *Ocean Modell.*, **16**, 141–159, https://doi.org/10.1016/j.ocemod.2006.08.005.

Chen, J., C. Meneveau, and J. Katz, 2006: Scale interactions of turbulence subjected to a straining relaxation destraining cycle. *J. Fluid Mech.*, **562**, 123–150, https://doi.org/10.1017/S0022112006000905.

Chen, R., G. R. Flierl, and C. Wunsch, 2014: A description of local and nonlocal eddy–mean flow interaction in a global eddy-permitting state estimate. *J. Phys. Oceanogr.*, **44**, 2336–2352, https://doi.org/10.1175/JPO-D-14-0009.1.

Chen, S., R. E. Ecke, G. L. Eyink, X. Wang, and Z. Xiao, 2003: Physical mechanism of the two-dimensional enstrophy cascade. *Phys. Rev. Lett.*, **91**, 214501, https://doi.org/10.1103/PhysRevLett.91.214501.

Chow, Y.-C., O. Uzol, J. Katz, and C. Meneveau, 2005: Decomposition of the spatially filtered and ensemble averaged kinetic energy, the associated fluxes and scaling trends in a rotor wake. *Phys. Fluids*, **17**, 085102, https://doi.org/10.1063/1.1990206.

Domaradzki, J. A., and D. Carati, 2007: A comparison of spectral sharp and smooth filters in the analysis of nonlinear interactions and energy transfer in turbulence. *Phys. Fluids*, **19**, 085111, https://doi.org/10.1063/1.2760281.

Dukowicz, J. K., and R. D. Smith, 1994: Implicit free-surface method for the Bryan-Cox-Semtner ocean model. *J. Geophys. Res.*, **99**, 7991–8014, https://doi.org/10.1029/93JC03455.

Emery, W. J., and R. E. Thomson, 2001: *Data Analysis Methods in Physical Oceanography.* 2nd ed. Elsevier Science, 638 pp.

Evans, L. C., 2010: *Partial Differential Equations.* 2nd ed. American Mathematical Society, 749 pp.

Eyink, G. L., 1995a: Local energy flux and the refined similarity hypothesis. *J. Stat. Phys.*, **78**, 335–351, https://doi.org/10.1007/BF02183352.

——, 1995b: Exact results on scaling exponents in the 2D enstrophy cascade. *Phys. Rev. Lett.*, **74**, 3800–3803, https://doi.org/10.1103/PhysRevLett.74.3800.

——, 1995c: Besov spaces and the multifractal hypothesis. *J. Stat. Phys.*, **78**, 353–375, https://doi.org/10.1007/BF02183353.

——, 2005: Locality of turbulent cascades. *Physica D*, **207**, 91–116, https://doi.org/10.1016/j.physd.2005.05.018.

——, 2008: Dissipative anomalies in singular Euler flows. *Physica D*, **237**, 1956–1968, https://doi.org/10.1016/j.physd.2008.02.005.

——, and H. Aluie, 2009: Localness of energy cascade in hydrodynamic turbulence. I. Smooth coarse graining. *Phys. Fluids*, **21**, 115107, https://doi.org/10.1063/1.3266883.

Fang, L., and N. T. Ouellette, 2016: Advection and the efficiency of spectral energy transfer in two-dimensional turbulence. *Phys. Rev. Lett.*, **117**, 104501, https://doi.org/10.1103/PhysRevLett.117.104501.

Ferrari, R., and C. Wunsch, 2009: Ocean circulation kinetic energy: Reservoirs, sources, and sinks. *Annu. Rev. Fluid Mech.*, **41**, 253–282, https://doi.org/10.1146/annurev.fluid.40.111406.102139.

Frisch, U., 1995: *Turbulence: The Legacy of A. N. Kolmogorov.* Cambridge University Press, 296 pp.

Gaube, P., D. B. Chelton, R. M. Samelson, M. G. Schlax, and L. W. O'Neill, 2015: Satellite observations of mesoscale eddy-induced Ekman pumping. *J. Phys. Oceanogr.*, **45**, 104–132, https://doi.org/10.1175/JPO-D-14-0032.1.

Germano, M., 1992: Turbulence: The filtering approach. *J. Fluid Mech.*, **238**, 325–336, https://doi.org/10.1017/S0022112092001733.

Gill, A. E., J. Green, and A. J. Simmons, 1974: Energy partition in large-scale ocean circulation and production of mid-ocean eddies. *Deep-Sea Res. Oceanogr. Abstr.*, **21**, 499–528, https://doi.org/10.1016/0011-7471(74)90010-2.

Gnanadesikan, A., R. D. Slater, P. S. Swathi, and G. K. Vallis, 2005: The energetics of ocean heat transport. *J. Climate*, **18**, 2604–2616, https://doi.org/10.1175/JCLI3436.1.

Kang, D., and E. N. Curchitser, 2015: Energetics of eddy–mean flow interactions in the Gulf Stream region. *J. Phys. Oceanogr.*, **45**, 1103–1120, https://doi.org/10.1175/JPO-D-14-0200.1.

Kelley, D. H., and N. T. Ouellette, 2011: Spatiotemporal persistence of spectral fluxes in two-dimensional weak turbulence. *Phys. Fluids*, **23**, 115101, https://doi.org/10.1063/1.3657086.

Kraichnan, R. H., 1964: Kolmogorov's hypotheses and Eulerian turbulence theory. *Phys. Fluids*, **7**, 1723–1734, https://doi.org/10.1063/1.2746572.

Krantz, S. G., 1999: *A Panorama of Harmonic Analysis.* Mathematical Association of America, 368 pp.

Leonard, A., 1974: Energy cascade in large-eddy simulations of turbulent fluid flows. *Advances in Geophysics*, Vol. 18, Academic Press, 237–248, https://doi.org/10.1016/S0065-2687(08)60464-1.

Levitus, S., 1982: *Climatological Atlas of the World Ocean*. NOAA Prof. Paper 13, 173 pp. and 17 microfiche.

Liao, Y., and N. T. Ouellette, 2015: Long-range ordering of turbulent stresses in two-dimensional flow. *Phys. Rev.*, **91E**, 063004, https://doi.org/10.1103/PhysRevE.91.063004.

Lindborg, E., 2006: The energy cascade in a strongly stratified fluid. *J. Fluid Mech.*, **550**, 207–242, https://doi.org/10.1017/S0022112005008128.

Liu, S., C. Meneveau, and J. Katz, 1994: On the properties of similarity subgrid-scale models as deduced from measurements in a turbulent jet. *J. Fluid Mech.*, **275**, 83–119, https://doi.org/10.1017/S0022112094002296.

Maddison, J. R., and D. P. Marshall, 2013: The Eliassen–Palm flux tensor. *J. Fluid Mech.*, **729**, 69–102, https://doi.org/10.1017/jfm.2013.259.

Meneveau, C., 1994: Statistics of turbulence subgrid-scale stresses: Necessary conditions and experimental tests. *Phys. Fluids*, **6**, 815–833, https://doi.org/10.1063/1.868320.

Molemaker, M. J., and J. C. McWilliams, 2010: Local balance and cross-scale flux of available potential energy. *J. Fluid Mech.*, **645**, 295–314, https://doi.org/10.1017/S0022112009992643.

Nikurashin, M., G. K. Vallis, and A. Adcroft, 2013: Routes to energy dissipation for geostrophic flows in the Southern Ocean. *Nat. Geosci.*, **6**, 48–51, https://doi.org/10.1038/ngeo1657.

O'Neill, L. W., D. B. Chelton, and S. K. Esbensen, 2012: Covariability of surface wind and stress responses to sea surface temperature fronts. *J. Climate*, **25**, 5916–5942, https://doi.org/10.1175/JCLI-D-11-00230.1.

Pacanowski, R. C., and S. G. H. Philander, 1981: Parameterization of vertical mixing in numerical models of tropical oceans. *J. Phys. Oceanogr.*, **11**, 1443–1451, https://doi.org/10.1175/1520-0485(1981)011<1443:POVMIN>2.0.CO;2.

Pearson, B., B. Fox-Kemper, S. Bachman, and F. Bryan, 2017: Evaluation of scale-aware subgrid mesoscale eddy models in a global eddy-rich model. *Ocean Modell.*, **115**, 42–58, https://doi.org/10.1016/j.ocemod.2017.05.007.

Piomelli, U., W. H. Cabot, P. Moin, and S. Lee, 1991: Subgrid-scale backscatter in turbulent and transitional flows. *Phys. Fluids*, **3A**, 1766–1771, https://doi.org/10.1063/1.857956.

Pope, S. B., 2000: *Turbulent Flows*. Cambridge University Press, 771 pp.

Rhines, P. B., 1975: Waves and turbulence on a beta-plane. *J. Fluid Mech.*, **69**, 417–443, https://doi.org/10.1017/S0022112075001504.

Ringler, T., M. Petersen, R. L. Higdon, D. Jacobsen, P. W. Jones, and M. Maltrud, 2013: A multi-resolution approach to global ocean modeling. *Ocean Modell.*, **69**, 211–232, https://doi.org/10.1016/j.ocemod.2013.04.010.

Rivera, M. K., W. B. Daniel, S. Y. Chen, and R. E. Ecke, 2003: Energy and enstrophy transfer in decaying two-dimensional turbulence. *Phys. Rev. Lett.*, **90**, 104502, https://doi.org/10.1103/PhysRevLett.90.104502.

——, H. Aluie, and R. E. Ecke, 2014: The direct enstrophy cascade of two-dimensional soap film flows. *Phys. Fluids*, **26**, 055105, https://doi.org/10.1063/1.4873579.

Sadek, M. M., H. Aluie, G. K. Vallis, and M. W. Hecht, 2017: Filtering the ocean: New insights into the baroclinic instability. *21st Conf. on Atmospheric and Oceanic Fluid Dynamics*, Portland, OR, Amer. Meteor. Soc., **119**, https://ams.confex.com/ams/21Fluid19Middle/webprogram/Paper318919.html.

Salmon, R., 1978: Two-layer quasi-geostrophic turbulence in a simple special case. *Geophys. Astrophys. Fluid Dyn.*, **10**, 25–52, https://doi.org/10.1080/03091927808242628.

——, 1980: Baroclinic instability and geostrophic turbulence. *Geophys. Astrophys. Fluid Dyn.*, **15**, 167–211, https://doi.org/10.1080/03091928008241178.

Scott, R. B., and F. Wang, 2005: Direct evidence of an oceanic inverse kinetic energy cascade from satellite altimetry. *J. Phys. Oceanogr.*, **35**, 1650–1666, https://doi.org/10.1175/JPO2771.1.

Smith, K. S., and G. K. Vallis, 2002: The scales and equilibration of midocean eddies: Forced–dissipative flow. *J. Phys. Oceanogr.*, **32**, 1699–1720, https://doi.org/10.1175/1520-0485(2002)032<1699:TSAEOM>2.0.CO;2.

Smith, R. D., M. E. Maltrud, F. O. Bryan, and M. W. Hecht, 2000: Numerical simulation of the North Atlantic Ocean at 1/10°. *J. Phys. Oceanogr.*, **30**, 1532–1561, https://doi.org/10.1175/1520-0485(2000)030<1532:NSOTNA>2.0.CO;2.

Sogge, C. D., 2008: *Fourier Integrals in Classical Analysis.* Cambridge University Press, 252 pp.

Speziale, C. G., 1985: Galilean invariance of subgrid-scale stress models in the large-eddy simulation of turbulence. *J. Fluid Mech.*, **156**, 55–62, https://doi.org/10.1017/S0022112085001987.

Stein, E. M., and G. Weiss, 1971: *Introduction to Fourier Analysis on Euclidean Spaces.* Princeton University Press, 297 pp.

Strichartz, R. S., 2003: *A Guide to Distribution Theory and Fourier Transforms.* World Scientific, 226 pp.

Talley, L. D., G. L. Pickard, W. J. Emery, and J. H. Swift, 2011: *Descriptive Physical Oceanography: An Introduction.* Academic Press, 555 pp.

Tao, B., J. Katz, and C. Meneveau, 2002: Statistical geometry of subgrid-scale stresses determined from holographic particle image velocimetry measurements. *J. Fluid Mech.*, **457**, 35–78, https://doi.org/10.1017/S0022112001007443.

Thuburn, J., H. Weller, H. G. Weller, G. K. Vallis, R. J. Beare, and M. Whitall, 2018: A framework for convection and boundary layer parameterization derived from conditional filtering. *J. Atmos. Sci.*, https://doi.org/10.1175/JAS-D-17-0130.1, in press.

Tulloch, R., J. Marshall, C. Hill, and K. S. Smith, 2011: Scales, growth rates, and spectral fluxes of baroclinic instability in the ocean. *J. Phys. Oceanogr.*, **41**, 1057–1076, https://doi.org/10.1175/2011JPO4404.1.

Vallis, G. K., 2006: *Atmospheric and Oceanic Fluid Dynamics.* Cambridge University Press, 745 pp.

von Storch, J.-S., C. Eden, I. Fast, H. Haak, D. Hernández-Deckers, E. Maier-Reimer, J. Marotzke, and D. Stammer, 2012: An estimate of the Lorenz energy cycle for the World Ocean based on the STORM/NCEP simulation. *J. Phys. Oceanogr.*, **42**, 2185–2205, https://doi.org/10.1175/JPO-D-12-079.1.

Vreman, B., B. Geurts, and H. Kuerten, 1994: Realizability conditions for the turbulent stress tensor in large-eddy simulation. *J. Fluid Mech.*, **278**, 351–362, https://doi.org/10.1017/S0022112094003745.

Waterman, S., and S. R. Jayne, 2011: Eddy-mean flow interactions in the along-stream development of a western boundary current jet: An idealized model study. *J. Phys. Oceanogr.*, **41**, 682–707, https://doi.org/10.1175/2010JPO4477.1.

Young, W. R., 2012: An exact thickness-weighted average formulation of the Boussinesq equations. *J. Phys. Oceanogr.*, **42**, 692–707, https://doi.org/10.1175/JPO-D-11-0102.1.

Youngs, M. K., A. F. Thompson, A. Lazar, and K. J. Richards, 2017: ACC meanders, energy transfer, and mixed barotropic–baroclinic instability. *J. Phys. Oceanogr.*, **47**, 1291–1305, https://doi.org/10.1175/JPO-D-16-0160.1.

Zanna, L., P. Porta Mana, J. Anstey, T. David, and T. Bolton, 2017: Scale-aware deterministic and stochastic parametrizations of eddy-mean flow interaction. *Ocean Modell.*, **111**, 66–80, https://doi.org/10.1016/j.ocemod.2017.01.004.